Maize *(Zea mays* L.) interaction with the arbuscular mycorrhizal fungus *Rhizophagus irregularis* allows mitigation of nitrogen deficiency stress: physiological and molecular characterization

Authors :

Bérengère Decouard[1], Niaz Bahar Chowdhury[2], Aurélien Saou[3], Martine Rigault[1], Isabelle Quilleré[1], Thomas Sapir[1], Anne Marmagne[1], Christine Paysant le Roux[4], Alexandra Launay-Avon[4], Florence Guerard[4], Caroline Mauve[4], Bertrand Gakière[4], Céline Lévy-Leduc[3], Pierre Barbillon[3], Rajib Saha [2], Pierre-Emmanuel Courty[5], Daniel Wipf[5], Bertrand Hirel[1], Alia Dellagi[1]*

1 : Université Paris-Saclay, INRAE, AgroParisTech, Institut Jean-Pierre Bourgin (IJPB), 78000, Versailles, France.

2 : Chemical and Biomolecular Engineering, University of Nebraska-Lincoln, Lincoln, NE, United States of America

3 : Université Paris-Saclay, AgroParisTech, INRAE, UMR MIA Paris-Saclay, 91120 Palaiseau,

France

4 : Université Paris-Saclay, CNRS, INRAE, Université Evry, Institute of Plant Sciences Paris-Saclay (IPS2), 91190, Gif sur Yvette, France. Université Paris Cité, CNRS, INRAE, Institute of Plant Sciences Paris-Saclay (IPS2), 91190, Gif sur Yvette, France

5 : Agroécologie, AgroSup Dijon, Centre National de la Recherche Scientifique (CNRS), Université de Bourgogne, Institut National de Recherche pour l'Agriculture, l'Alimentation, et l'Environnement (INRAE), Université Bourgogne Franche-Comté, Dijon, France.

* Correspondance:

Prof. Alia Dellagi

Address: Université Paris-Saclay, INRAE, AgroParisTech, Institut Jean-Pierre Bourgin (IJPB), 78000, Versailles, France.

Phone: +33 1 30 83 32 28

E-mail: alia.dellagi@agroparistech.fr

Key words: N use efficiency; Nitrogen uptake; arbuscular mycorrhizal fungi, Maize, metabolic modelling.

Abstract

Maize is currently the most productive cereal crop in the world (www.faostat.org). Maize can form a symbiotic relationship with the Arbuscular Mycorrhizal Fungus MF, *Rhizophagus irregularis*. In this relationship, the fungus provides the plant with additional water and mineral nutrients, while the plant supplies carbon compounds to the fungus. Two maize lines were studied, and they exhibited contrasting responses to AMF inoculation based on their physiological and molecular characteristics. Interestingly, the beneficial effects of the AMF were observed mainly under conditions of limited N fertilization. Under such conditions, the AMF helped maintain plant biomass production even when there was a significant reduction in N supply. The availability of nitrogen was found to be a crucial factor influencing all the traits studied. This suggests that the level of N supply plays a pivotal role in determining how the maize plants interact with the AMF. Despite the two maize lines showing different transcriptomic and metabolomic responses to *R. irregularis*, their agro-physiological traits remained similar. This indicates that while there may be genetic differences in how the plants respond at the molecular level, the overall growth and productivity outcomes are comparable. Both the plant and fungal transcriptomes were more significantly influenced by the level of N nutrition rather than the specific maize genotype. This suggests that N availability has a more profound impact on gene expression in both organisms than the genetic makeup of the maize plant. To understand the metabolic implications of this symbiotic relationship, we integrated transcriptomic data into a multi-organ Genome-scale metabolic model (GSM) called iZMA6517 based on a stoichiometric approach. This modelling approach highlighted nucleotide and ureides metabolism as previously unrecognized factors contributing to the symbiotic N nutrition facilitated by *R. irregularis*, thereby enhancing maize growth.

Introduction

Nitrogen (N) is the fourth most abundant component of plant biomass, which explains its pivotal role in agriculture (Hirel *et al.*, 2011; Hirel and Krapp, 2020). Indeed large inputs of N fertilizers are necessary to ensure optimal crop productivity (Hirel *et al.*, 2007, 2011). However, only 30 to 50% of the N available in the soil is taken up by most crops, resulting in important N losses which can cause damage to the environment such as water pollution and increased greenhouse effect (Schlesinger, 2009; Lassaletta *et al.*, 2016). It is urgent to minimize these impacts while simultaneously meeting the increasing demand for food production resulting from population growth. Ensuring crop productivity while minimizing N supply can be monitored by measuring nitrogen use efficiency (NUE). A better understanding of how to enhance NUE is a major challenge in the context of agroecology as it represents the capacity of the plant to produce grains or vegetative biomass per unit of available N (Hirel *et al.*, 2007; Lea and Miflin, 2018; Wang *et al.*, 2018; Liu *et al.*, 2022). Three physiological processes contribute to NUE: (Masclaux-Daubresse *et al.*, 2010; Lea and Miflin, 2018) : 1) N uptake efficiency involved in aquisition N from the soil by means of root-specific inorganic or organic N transporters (Fan *et al.*, 2017; Wang *et al.*, 2018); 2) N assimilation efficiency which is the incorporation of inorganic N into organic N-containing molecules necessary for plant growth and development (Hirel *et al.*, 2011; Hirel and Krapp, 2020; Wani *et al.*, 2021); and 3) N remobilization efficiency which represents the capacity of the plant to remobilize N and transfer it to storage organs (Masclaux-Daubresse *et al.*, 2010; Kant, 2018). Direct uptake of minerals including N and P from the soil by plants is ensured by transporters known to drive the so called “direct transport”. Interstingly, to fulfil their N-associated metabolic needs, plants can establish symbiosis with beneficial soil microbes which help to improve their N nutrition by different mechanisms, some of which are well characterized. Exploiting the capacity of a crop to benefit from beneficial microbes in terms of N nutrition in order to maintain yields while reducing chemically synthesized N input is challenging in the

context of a more sustainable agriculture (Gianinazzi *et al.*, 2010; Verzeaux *et al.*, 2017; Wipf *et al.*, 2019; Dellagi *et al.*, 2020; Gojon, 2022; Xie *et al.*, 2022).

The best characterized symbiosis which improves legume N nutrition occurs when symbiotic bacteria from the Rhizobiaceae family allows fixation of atmospheric N_2 and its reduction to NH_4^+ readily usable by the host plant (Udvardi and Poole, 2013; Masson-Boivin and Sachs, 2018). Nitrogen can also be transferred from the soil to the roots when the plant is colonized by Arbuscular Mycorrhizal Fungi (AMFs), a symbiotic process occurring in 80% of land plants including cereals (Gianinazzi *et al.*, 2010; Chen *et al.*, 2018*a*; Gojon, 2022; Xie *et al.*, 2022). AMFs are obligate biotrophs, meaning that they rely on their living host plants to complete their life cycle. The early steps of AMF symbiosis involve signal exchange between the host roots of the host plant and the fungus. This signalling process leads to establishment of a physical contact between the partners during which the fungus develops structures like a hyphopodium on the root epidermal cell followed by its growth inside these cells up to the cortical cells where it differentiates into highly branched structures called “arbuscules”. Around these arbuscules, the cortical cells undergo strong reorganization leading to the formation of a structure called “periarbuscular membrane” (PAM). Dual nutritional exchange occurs at the interface of this membrane where the transfer of carbon containing molecules derived from photosynthesis such as hexoses and lipids feed the fungus, which in turn provides minerals such as N and P (Smith and Read, 2002; Gianinazzi *et al.*, 2010; MacLean *et al.*, 2017; Choi *et al.*, 2018; Dellagi *et al.*, 2020). The extra-radical mycelium which represents an extension of the arbuscular structures, allows the fungus to explore the surrounding rhizosphere and to take up minerals further translocated to the periarbuscular interface to be finally delivered to the host plant. In many case, an AMF symbiotic association is able to increase tolerance to abiotic and biotic stresses (Choi *et al.*, 2018; Berger and Gutjahr, 2021).

It is well established that phosphorus (P) deficiency is the main driver for the establishment of mycorrhizal symbiotic associations (Breuillin *et al.*, 2010; Smith *et al.*, 2011; Balzergue *et*

al., 2013; Wang *et al.*, 2017; Paries and Gutjahr, 2023). Phosphorus deficiency triggers exudation from roots of signaling molecules such as strigolactones that stimulate AMF hyphal branching (Lanfranco *et al.*, 2018; Hull *et al.*, 2021). In addition, isotope tracing experiments have shown that AMF provide phosphorus to their hosts (Sawers *et al.*, 2017; Das *et al.*, 2022). In contrast, the benefit of a mycorrhizal symbiosis in terms of N uptake and utilization by the host plant, remains to be fully characterized (Chen *et al.*, 2018*a*; Dellagi *et al.*, 2020; Gojon, 2022; Xie *et al.*, 2022). It is known that N can be transported to the plant by AMF (Courty *et al.*, 2015; Garcia *et al.*, 2016; Chen *et al.*, 2018*a*). Two transporters that mediate the mycorrhizal N transport pathway have been identified so far. For example, in rice, a transporter specifically involved in the transfer of nitrate to the roots of the host plant via the AMF has been described (Wang *et al.*, 2020). In maize, an ammonium transporter enabling the uptake of inorganic N has recently been characterised (Hui *et al.*, 2022).

Maize is currently the most productive cereal crop in the world (www.faostat.org) with a global yield exceeding that of rice (Liu *et al.*, 2020). Maize is grown for several purposes including animal feed, food and biotechnological applications (Ranum *et al.*, 2014; Revilla *et al.*, 2022). Different maize genotypes are able to develop a symbiotic association with AMF (Sawers *et al.*, 2018*a*; Berger and Gutjahr, 2021). Several studies have shown that AMF can supply substantial amount of N to maize (Quiroga *et al.*, 2020; Hui *et al.*, 2022). However, physiological and molecular characterization of maize's interaction with AMF under different N supply levels has never been undertaken. We reasoned that utilizing AMF to reduce N fertilization requires investigating the maize physiological responses to AMF under different levels of N fertilization. In the present study, we have studied in an integrated manner the impact of N nutrition on the interaction between maize and the AMF *Rhizophagus irregularis* both at the physiological and molecular levels. Using phenotyping, transcriptomic and metabolomic approaches, we have characterized such interaction using two maize lines which benefit from symbiotic association with the fungus in terms of agronomic performance. Genome-scale metabolic modeling (GSM) is a computational tool to model plant metabolism and can highlight potential key metabolic pathways in plant in response to environmental

cues (Morris *et al.*, 2023). Initial efforts on maize metabolic models were limited to its leaf (Simons *et al.*, 2014) and root (Chowdhury *et al.*, 2022*b*) GSMs, which showed excellent agreement with existing literature regarding phenotypical predictions. Most recently, a multi-organ GSM of maize line B73, *i*ZMA6517 (Chowdhury *et al.*, 2023), is proposed which includes full scale GSMs of root, stalk, kernel, and leaf; connected via phloem tissue. *i*ZMA6517 predicted organ-specific metabolic bottlenecks accurately and explored symbiotic relationship with *R. irregularis*. Thereby, apart from experimental works, we used *i*ZMA6517 to predict plant agronomic performance. Interestingly, *i*ZMA6517 identified purine and pyrimidine biosynthetic pathways as key physiological processes involved in the efficiency of N utilization in the symbiotic association.

Material and methods

Plant material, growth conditions and inoculation

The maize inbred lines used in this study B73 and Lo3 are described in Supplementary table 1. The reference maize genotype B73, for which the genome was fully sequenced, represents the reference genome for the maize species (Schnable *et al.*, 2009). Additionally, B73 is known be responsive to AMF, resulting in increased biomass (Ramírez-Flores *et al.*, 2019; Berger and Gutjahr, 2021). Lo3, was selected due to its enhanced biomass response following inoculation with *R. irregularis.* This selection was based on the outcomes of two rounds of screening aimed at identifying maize lines that exhibit increased biomass in the presence of AMF under limiting N conditions. These screening round were performed on the core collection previously described (Cañas *et al.*, 2017). The purpose was to identify maize genotypes which benefits from AMF inoculation (data not shown). The fungal strain used is the highest quality of purity strain *Rhizophagus irregularis* DAOM197198 (Agronutrition, Toulouse, France). Inoculum was prepared in distilled water and the required volume of spore suspension was added next to the germinated seed or plantlet with a pipette.

In all experiments, seeds were surface-sterilized as follows. Seeds were first incubated in ethanol for 5 minutes at 28°C followed by rinsing with distilled water. Then they were incubated for 45 minutes in a 15% commercial bleach solution with 0.01% Triton x100 then rinsed in distilled water. They were placed on wet sterile Whatman paper in Petri dishes closed with parafilm and incubated in the dark for 48-72h at 20°C. Germinated seeds were selected and then sown in pots of 4 litres containing a mix of sterilized unfertilized peat (40% Baltic blond peat 0-10 mm, 60% Brown peat 0-10 mm, 75 g oligoelements, pH $CaCl_2$ 5.3 – 5.8, Stender, France) and dried clay beads (reference: 17831050 BILLE ARGILE LIA 8/16, Soufflet, France) 1:1/v:v. The experimental design and the different steps of growing and harvesting of the experiment in 2020 and 2021 are presented in Supplementary Figure 1 and 2 respectively. Meteorological conditions within the greenhouse during 2020 are depicted in Supplementary Figure 3. For each condition 9-10 plants were used. Three inoculations with spores of *R. irregularis* were performed as follow: The first inoculation with 500 spores/plant at sowing, second inoculation 1 week after sowing with 200 spores/plant and a third inoculation 2 weeks after sowing with 200 spores/plant. Control plants were treated with distilled water. Plants were grown under three different nitrogen regimes: low N (LN, 1mM NO_3^-), medium N (MN, 5 mM NO_3^-) and high N (HN, 10 mM NO_3^-). The specific composition of these regimes is provided in Supplementary Table 2. For each N regime, plants were irrigated for the first three weeks with the solution corresponding to the chosen N regime with low P (named P-) containing 10 µM phosphate in order to trigger AMF colonization. Then, at dates indicated in Supplementary Figure 1 and 2, irrigation was changed to the same N level but 300 µM P (named P+, Supplementary Table 2). Increasing P level in the irrigation solution was necessary to allow plants reach the maturity stage. To determine ^{15}N uptake, ^{15}N labelling was performed at indicated dates (Supplementary Figure 1). 100 mL of 45 mM KNO_3 solution enriched at 2% ^{15}N was applied to each plant in order to provide 1,25mg of ^{15}N.

Harvesting procedures

Plants grown in 2020 were used for the phenotyping, metabolomics, RNA-seq and RT-qPCR experiments. Plants grown in 2021 were to monitor fungal colonization and RT-qPCR experiments. For RNA and metabolite extractions, leaf and root samples were harvested and frozen in liquid nitrogen before RNA extraction. Depending on the experiment and the biological question asked, one, two or three developmental stages were chosen for tissue harvesting. Those stages were determined based a combination of two criteria: (i) the presence of arbuscular symbiotic structures in maize roots and (ii) plant developmental stages. The first one is the vegetative stage (VS) corresponding to the 7- to 8-leaf stage (Cañas *et al.*, 2017). This stage is an indicator of a highly metabolically and photosynthetically active leaf tissue but only few fungal structures start to be visible in roots. The second stage corresponds to 15 days after the Vessel Tasselling stage (VT+15 stage) where root colonization is clearly established and plant is in the early phase of flowering. This stage was chosen because it allows harvesting roots without imposing too great a stress on the plant in order to make sure kernels are not affected. The third stage is maturity stage (MS) and corresponds to plants displaying mature ears. Dates of harvesting for VS, VT+15 stage and MS differed depending on the condition and the year of experiment (Supplementary Figure 1 and 2). For leaf tissues, harvesting consisted in cutting a piece of 1 cm x 10 cm of leaf mesophyll along the midrib from the 6th fully emerged leaf for the VS. For VT+15 stage and MS, a piece of 1 cm x 10 cm leaf surface from the leaf below the ear of each individual plant was harvested. The leaf below the ear was chosen for providing a good proxy of the sink-to-source transition during grain filling (Prioul and Schwebel-Dugué, 1992).

Roots were harvested at VS, VT+15 stage or MS depending on the type of experiment. For each treatment/condition, roots were collected from 5 plants. Thin secondary roots were harvested from the surrounding root system, close to the pot borders. They were washed with distilled water, then frozen in liquid nitrogen or stored in distilled water. Following root harvesting, the plants grown in 2020 were left to grow until maturity. Thus, the roots used for

the different omics analyses corresponded to the same plants as those that produced grains and were phenotyped for physio-agronomical traits.

Quantification of yield, biomass, C, N, ^{15}N and P

Plant organs were harvested then oven dried at 80°C for 3 to 5 days then ground to fine powder. Yield was quantified by weighing dry grains. Biomass of the aerial parts including stalks, leaves, and cobs were weighed after drying. The upper regions of the root system was harvested. This did not allow to quantify the whole root biomass since it was impossible but allowed to quantify the percentage of C, N and P. For each plant and each organ, 5,000 µg of dry powder was placed in tin capsules to quantify the total N and C concentrations using the FLASH 2000 Organic Elemental Analyzer (Thermo Fisher Scientific Villebon, France) and the ^{15}N enrichment using the Delta V Advantage isotope ratio mass spectrometer (Thermo Fisher Scientific, France). Supplementary Table 3 indicates the calculations of different traits with C and N content. A% (Atom percent) represents the ^{15}N enrichment in the sample [^{15}N/(total N)]. Since the natural ^{15}N abundance in N unlabeled samples was 0.3663 (A% control), specific enrichments due to the ^{15}N uptake were calculated as E% = (A% - 0.3363).The P concentration of shoots, grains and roots was measured using the molybdate blue method on a Shimadzu UV-160 spectrophotometer (Shimadzu Biotech) after acid digestion (Murphy and Riley, 1962).

Quantification of root colonization level by AMF structures

Thin secondary roots were harvested as indicated above and carefully washed in distilled water. They were incubated in 10% KOH overnight at room temperature. They were then rinsed in distilled water and incubated in 5% black ink (Sheaffer Skrip Bottled Ink, France) solution for 10 min at 70°C. Washing was performed by incubating roots in 8% acetic acid for 25 min. For the quantification of % of AM colonization (total, arbuscules, vesicles) 50 pieces of 1 cm length each were mounted on a slide for observation of AM structures under light

microscope using the slide method (Giovannetti and Mosse, 1980). Quantifications were performed on roots collected from 5 plants for each condition.

RNA extraction for RT qPCR and RNAseq

RNA extraction was performed with TRIzol (Thermo Fisher Scientific, USA) protocol. Fresh tissue of leaves or roots (100 mg) were frozen in liquid nitrogen then ground to fine powder that was homogenized in 1 mL of TRIzol. Two glass beads are added to the extract in the tube which was then vortexed for 5 minutes, then the samples were incubated for 5 minutes at room temperature (RT). Two hundred microliters of chloroform were added then the sample was vortexed for 5 minutes and incubated 3 minutes at RT. Samples are centrifuged at 12,000 g for 15 minutes at 4°C. The aqueous phase (approximately 500 µL) was transferred to a new tube with an equal volume of ethanol (100%). Samples mixed with ethanol were then transferred to a column (Zymo-Spin™ IC, Germany); for purification following manufacturer's instructions.

cDNA synthesis and RT-PCR

1 µg of RNA was first treated with DNAse (Thermo Fisher Scientific, USA) in a 10 µL total volume. 1 µg of DNAse treated RNA was then used for reverse transcription using oligo-dT and the reverse trancriptase Revert aid (Thermo Fisher Scientific, USA) following the manufacturer's instructions. Quantitative PCR reactions were carried out as described (Verly *et al.*, 2020). For each sample, a cycle threshold (Ct) value was determined and converted into Starting Quantity (SQ) also named Arbitrary Units (AU) values based on a standard curve equation. The AU values obtained for each gene of interest was then divided by the mean of AU values obtained for the chosen reference gene (indicated in each dataset) leading to the normalized transcript level value. Primer sequences are described in Supplementary table 4.

RNAseq and Bioinformatic Analysis

RNA-seq libraries were constructed by the POPS platform (IPS2) using the Illumina Stranded mRNA Prep kit (Illumina®, California, U.S.A.) according to the supplier's instructions. Libraries were sequenced by the Genoscope (Évry-Courcouronnes, France) on a Novaseq 6000 instrument (Illumina) with 150 base paired-end sequences.

Raw Data cleaning

The raw data were treated as follow:

1- Illumina filter. Performed as described with chastity cutoff of 0,6.

To remove the least reliable data from the analysis, the raw data were filtered to remove any clusters that have "too much" intensity corresponding to bases other than the called base. The purity of the signal from each cluster was examined over the first 25 cycles and calculated as Chastity = Highest_Intensity / (Highest_Intensity + Next_Highest_Intensity) for each cycle. The default filtering implemented at the base calling stage allows at most one cycle that is less than the Chastity threshold (0,6).

2- Genoscope filter. An in-house procedure was used in order to remove adapters and primers on the whole read and low-quality nucleotides from both ends (while quality value is lower than 20) and then continue next steps with the longest sequence without adapters and low-quality bases. Remove sequences between the second unknown nucleotide (N) and the end of the read. This step is done on trimmed (adapters + quality) reads. Discard reads shorter than 30 nucleotides after trimming. Remove read pairs that come from the low-concentration spike-in library of Illumina PhiX Control. Reads pairs corresponding to ribosomal RNA were removed using sortMeRNA (v2.1, (Kopylova *et al.*, 2012).

These previous two steps were performed by the sequencing facility at Genoscope. Cleaned reads from Genoscope were adapter trimmed again by the POPS platform with BBduk from the BBmap suite (v38.84, Bushnell, 2014) with the options k=23 ktrim=r qtrim=r

useshortkmers=t mink=11 trimq=20 hdist=1 tpe tbo minlen=30 using adapter sequences file included in the BBTools package.

Mapping and Gene expression quantification

Filtered reads were then mapped and counted using STAR (v2.7.3a, (Dobin *et al.*, 2013)) with the following parameters --alignIntronMin 5 --alignIntronMax 60000 --outSAMprimaryFlag AllBestScore --outFilterMultimapScoreRange 0 --outFilterMultimapNmax 20 on a combined reference genome made by concatenating the files of the *Zea mays* B73 (V4.49) and *Rhizophagus irregularis* (V2) reference genomes and the associated GTF annotation files (also combined). Between 75.3 and 96.1 % of the reads were uniquely mapped (median = 91.9%). Between 68 and 88 % of the reads were associated to annotated genes (median = 85.3%).

Statistical Analyses of Expression Data

Statistical analyses were conducted on R v3.6.2 (R Core Team, 2020) using the script-based tool DiCoExpress (Lambert *et al.*, 2020; AU - Baudry *et al.*, 2022). DiCoexpress used the Bioconductor package edgeR (v 3.28.0, (Robinson *et al.*, 2010; McCarthy *et al.*, 2012).The raw count file used for the statistical analyses only contain the reads of the *Zea mays* organism. Dicoexpress DiCoExpress analyse RNAseq projects with at most two biological factors. For this reason and to answer biological questions of interest, 4 separate statistical analyses were conducted on samples from (I) B73 leaves, (ii) B73 roots, (iii) Lo3 leaves, (iv) Lo3 roots.

Gene Filtering and Normalization

For the four analyses, low counts genes giving low counts were filtered using the “FilterByExpression” feature available through the edgeR package with a minimum count threshold of 15. Raw counts were normalized with the trimmed mean of M values (TMM) method implemented in edgeR package.

Differential Expression Analysis

The differential analysis is based on a negative binomial generalized linear model. For the 4 *Zea mays* analyses, the log2 of the average normalized gene expression is an additive function of a condition effect (LN or HN), a treatment effect (Rhizo equivalent to *R. irregularis* inoculation) or Ctrl (equivalent to control treatment), an interaction between the condition and the treatment and the technical replicate factor (3 modalities). To make the processing of these multifactorial designs easier, Differential Expression (DE) analyses were performed using the DiffAnalysis_edgeR function of DiCoExpress to generate automatically the contrasts. In each analysis, we considered the difference between the two treatments at each condition and averaged on the two conditions, the difference between the two conditions given a treatment and averaged on the two treatments and the interaction effect defined as the difference between the two treatments at a given condition (HN) minus the difference between the two treatments at the second condition (LN). It leads to a total of 8 contrasts per analysis and only biologically meaningful contrasts were interpreted. For each contrast a likelihood ratio test was applied and raw p-values were adjusted with the Benjamini–Hochberg procedure to control the false discovery rate. The distribution of the resulting p-values followed the quality criterion described by Rigaill et al. (Rigaill *et al.*, 2018). A gene was declared differentially expressed if its adjusted p-value was lower than 0.05.

For the fungal transcripts, expression ratios were considered relative to the N nutrition condition. Fungal transcripts displaying a FC higher or lower than 1.5 in LN compared to HN conditions were considered Each transcript ID was converted into the protein ID using the fungal genomic resource Mycocosm at the JGI website: https://mycocosm.jgi.doe.gov/pages/search-for-genes.jsf?organism=Rhiir2_1 (Tisserant *et al.*, 2013; Chen *et al.*, 2018*b*). Based on KOG (euKaryotic Orthologous Groups), functional classes to which the genes belong were determined Over-represented functional KOG categories of these fungal genes were determined using the 'KOGMWU' 1.2 R package

(Date 2019-02-19. Author Mikhail V. Matz). The fold enrichment value is based on a Mann-Witney, U-test that uses for each gene, a combination of the FC and the KOG category.

Metabolomic analyses

All extraction steps were performed in 2 mL Safelock Eppendorf tubes. The ground dried samples (5 mg DW) were resuspended in 1 mL of frozen (-20°C) Water:Acetonitrile:Isopropanol (2:3:3) containing Ribitol at 4 mg/L and extracted for 10 min at 4°C with shaking at 1500 rpm in an Eppendorf Thermomixer. Insoluble material was removed by centrifugation at 13500 rpm for 10 min. 700 µL were collected and 70 µL of myristic acid d27 at 0.3 g/L was added as an internal standard for retention time locking. After centrifugation, aliquots of each extract (100 µL) were dried for 4 h at 35 °C in a Speed-Vac and stored at -80°C. Two Blank tubes underwent the same steps as the samples.

Sample derivatization and analysis : All steps of GC-MS analyses were done as described in Fiehn et al. (Fiehn, 2006; Fiehn *et al.*, 2008). Agilent literature PUB: 5989-8310EN (Agilent G1676AA Agilent Fiehn GC/MS Metabolomics RTL Library User Guide. June 2008. Agilent P/N: G1676-90000, Agilent Fiehn GC/MS Metabolomics RTL Library Product Note. May 2008). Samples were taken out of -80°C, warmed 15 min before opening and speed-vac dried again for 1 hour at 35 °C before adding 10 µl of 20 mg/mL methoxyamine in pyridine to the samples and the reaction was performed for 90 min at 30°C under continuous shaking in an Eppendorf thermomixer. 90 µL of N-methyl-N-trimethylsilyl-trifluoroacetamide (MSTFA) (REGIS TECHNOLOGIES 1-270590-200 -10x1g) were then added and the reaction continued for 30 min at 37°C. After cooling, 90 µL were transferred to an Agilent vial for injection.

4 hours after derivatization 1 µL of sample was injected in splitless mode on an Agilent 7890B gas chromatograph coupled to an Agilent 5977A mass spectrometer. The column was an ZORBAX DB5-MS from Agilent (30 m with 10 m integraguard column - ref 122-5532G). An injection in split mode with a ratio of 1:30 was systematically performed for saturated quantification compounds. Oven temperature ramp was 60 °C for 1 min then 10 °C/min to

325 °C for 10 min. Helium constant flow was 1.1 mL/min. Temperatures were as follows: injector: 250°C, transfer line: 290°C, source: 230 °C and quadripole 150 °C. The quadrupole mass spectrometer was switched on after a 5.90 min solvent delay time, scanning from 50-600 µ. Absolute retention times were locked to the internal standard d27-myristic acid using the RTL system provided in Agilent's Masshunter software. Retention time locking reduces run-to-run retention time variation. Samples were randomized. A fatty acid methyl esters mix (C8, C9, C10, C12, C14, C16, C18, C20, C22, C24, C26, C28, C30) was injected in the middle of the queue for external RI calibration.

Data processing and quantification: Raw Agilent datafiles were analyzed with AMDIS http://chemdata.nist.gov/mass-spc/amdis/. The Agilent Fiehn GC/MS Metabolomics RTL Library (version June 2008) was employed for metabolite identifications. This library is the most comprehensive library of metabolite GC/MS spectra that is commercially available. It contains searchable GC/MS EI spectra and retention time indexes from approximately 700 common metabolites. Peak areas determined with the Masshunter Quantitative Analysis (Agilent) in splitless and split 30 modes. Because automated peak integration was occasionally erroneous, integration was verified manually for each compound in all analyses. Resulting areas were compiled in one single Excel file for comparison. Peak areas were normalized to Ribitol and Dry Weight. Metabolite contents are expressed in arbitrary units (semi-quantitative determination).

Amino acid quantification by OPA-HPLC

Extraction procedure was identical that one described for metabolomics. Here 200µL of the extraction solution was taken and dried in a Speed-Vac evaporator for 2 h at 30°C before adding 1,3 mL of H_20 milliQ. The o-phtaldialdéhyde (OPA) reagent was made 48 h before first use by dissolving OPA at 12mg/mL in 200 µL of methanol and adding 1.8 mL of sodium borate 0.5M (pH 9.5) and 40 µL of 2-mercaptoethanol. The reagent was filtered into an autosampler vial and used for up to 3 days. Precolumn derivatization was performed in the injection loop by automated mixing of 10 µL sample and 10 µL OPA reagent, followed by a

delay of 2 min prior to injection. The HPLC (Alliance Waters 2695, Waters Corporation, Massachusetts, USA) fitted with a fluo detector (Multi λ Fluorescence Detector 2475) was used. Compounds were measured at λ excitation of 340 nm and λ emission of 455 nm. The chromatographic separation was performed with Symmetry C18 column (3.5µm, 4.6*150 mm) by gradient elution at 40 °C using buffer A (20% methanol, 80% sodium acetate, 1% tetrahydrofuran, pH 5.9) and buffer B (80% methanol, 20% sodium acetate, pH 5.9). Buffer flow rate was 0.8 mL/min throughout and total run time per injection was 42 min. The chromatography data were analysed by Empower software. Peak identity was confirmed by co-elution with authentic standards. Concentration was calculated with calibration curve using peak area of compound of interest.

Statistical analyses

All statistical analyses were performed with RStudio 2023.06.0+421 "Mountain Hydrangea" under the free software environment R version 4.3.1 (Beagle Scouts). All Anova were implemented with the “aov” R package. All heatmaps were generated with the estimated marginal means that were calculated using the R package “emmeans”. Heatmap for physio-agronomical traits was generated with ‘pheatmap’ 1.0.12 package (Date 2019-01-04. Author Raivo Kolde) by implementing the ward.D2 hierarchical clustering method (Murtagh and Legendre, 2014). Heatmap for physio-agronomical traits was generated with the ‘pheatmap’ R package 1.0.12 Date 2019-01-04 (Author Raivo Kolde). Heatmaps for metabolomics, including the interactive ones, were generated with “heatmaply” R package (Galili *et al.*, 2018)

Metabolomics data were analyzed with the R package MultiVarSel (Perrot-Dockès *et al.*, 2018) which is the implementation of the variable selection approach in the multivariate linear model proposed in (Perrot-Dockès et al., 2018a), theoretically analysed in (Perrot-Dockès et al., 2018b) and applied in several contexts of omics data analyses such as (Grandclaudon *et al.*, 2019; Perrot-Dockès *et al.*, 2022). The list of R packages used in this study: Chiquet J, Donnet S, Barbillon P (2023). *sbm: Stochastic Blockmodels*. R package version 0.4.5-9000,

<https://grosssbm.github.io/sbm/>. Kolde R (2019). _pheatmap: Pretty Heatmaps_. R package version 1.0.12, <https://CRAN.R-project.org/package=pheatmap>. Lenth R (2023). _emmeans: Estimated Marginal Means, aka Least-Squares Means_. R package version 1.8.6, <https://CRAN.R-project.org/package=emmeans>. Perrot-Dockès M, Lévy-Leduc C, Chiquet J. R package MultiVarSel available from the Comprehensive R Archive Network, 2017. <https://CRAN.R-project.org/package=MultiVarSel>.

Genome-Scale Metabolic Modelling (GSM) and Transcriptomics Data Integration

To investigate the metabolism of maize from systems level, we used *i*ZMA6517 as the template model(Chowdhury *et al.*, 2023). The model is specific to B73 genotype and consists of organ-specific GSMs of root, stalk, leaf, and kernel. All these individual organ GSMs are connected through a common phloem pool. The model has been described (Chowdhury *et al.*, 2023). The model was contextualized with HN Control, HN Rhizo, LN Control, and LN Rhizo using EXTREAM algorithm (Chowdhury *et al.*, 2023). The upper and lower bounds for the mentioned conditions are presented in the Supplementary Table 5. The General Algebraic Modeling System (GAMS) version 24.7.4 with IBM CPLEX solver was used to run FBA and FVA, E-Flux, and the FSA algorithm on the model. Each of the algorithms was scripted in GAMS and then run on a Linux-based high-performance cluster computing system at the University of Nebraska-Lincoln. Instructions for running files in GAMS through NEOS server have been published (Chowdhury *et al.*, 2022*a*). All the necessary files for COBRApy users can also be accessed through the *i*ZMA6517 publication (Chowdhury *et al.*, 2023).

Metabolic Bottleneck Analysis (MBA)

To determine the metabolic bottlenecks in each of HN Control, HN Rhizo, LN Control, and LN Rhizo conditions, we used Metabolic Bottleneck Analysis **(**MBA) (Chowdhury *et al.*, 2023). MBA expands the flux space of each reaction separately and assesses its impact on the whole plant biomass growth rate. Further details on MBA can be accessed in the original

publications. MBA pinpoints plant-wide metabolic bottlenecks, which were further analyzed for biological insights.

Results

The impact of *Rhizophagus irregularis* on maize growth and yield is strongly dependent on the level of N nutrition

To investigate the molecular and physiological mechanisms involved in maize interaction with AMF in terms of N nutrition and have an overview of the diversity of these mechanisms we used two AMF-responsive maize lines B73 and Lo3. In order to find at which level of N fertilization the two lines benefit most from the fungal inoculation, these were grown in a greenhouse under low N (LN), medium N (MN) or high N (HN) corresponding to 1 mM NO_3^-, 5 mM NO_3^- and 10 mM NO_3^- in the nutrient solution respectively. The impact of *R. irregularis* inoculation on maize physio-agronomic traits was monitored by measuring shoot biomass, grain yield, total N content and ^{15}N enrichment allowing the calculation of other traits such as NUE as described in Supplementary table 3. In inoculated plants, an increase in the shoot biomass production was only observed under LN in both lines, whereas an increase in grain yield only occurred in B73 (Figure 1A, 1B). A slight negative impact of *R. irregularis* inoculation was observed on B73 grain yield when plants were grown under HN. Interestingly, *R. irregularis* allowed inoculated plants grown under LN to produce a similar vegetative biomass compared to non-inoculated plants fed with 5 times more NO_3^-. However, AMF inoculation did not influence shoot biomass of either maize genotypes under MN or HN (Figure 1B).

In inoculated plants, an increase in NUE for grain was observed under LN and MN fertilization conditions only in B73 (Figure 1D). Aerial parts NUE increased only in LN conditions for both B73 and Lo3 (Figure 1C). Together, these data indicate that benefit from AMF in terms of maize yield and NUE is higher under limiting N supply than under ample N supply and depends on the genotype. When we examined the impact of the AMF on N

resource allocation under the three levels of N, a significant increase of biomass allocation to the grain was observed in both B73 and Lo3 only in LN (Figure 1E**)**. Chlorophyll quantities were monitored during the vegetative phase and were also increased by AMF inoculation under LN only (Figure 1F).

The grain N content, considered as a proportion relative to dry mass, remains consistent across genotype and the N feeding conditions. However, an exception to this trend is observed in the B73 genotype, where the N content is notably lower in inoculated LN and MN plants (Figure 2A). Both the shoot and the root N contents were roughly proportional to the amount of N provided to the plant. Fungal inoculation did not change N content under LN. However, under higher N supply levels, a significant increase in the N content of aerial parts was observed in response to *R. irregularis* under MN for B73 and under HN for Lo3 indicating that these lines are able to store higher levels of N in the vegetative parts upon association with the AMF even under ample N (Figure 2C). The C/N ratio exhibited minimal change, as a slight decrease in B73 inoculated LN plants aerial parts and increase in grains in response to *R. irregularis* under MN for B73 was observed (Figure 2G-H). Changes in carbon (C) content were not statistically significant.

To determine whether N uptake is modified during the symbiotic interaction, plants were labelled with a pulse of ^{15}N provided at the vegetative stage. The total quantity of ^{15}N in aerial parts and grains measured at maturity is unchanged whatever the treatment (Supplementary Figure 4). These data indicate that the fungus does not affect N uptake at the vegetative stage. However, under LN conditions, ^{15}N-enrichment in the different organs of the inoculated plants was much lower than in control plants for both B73 and Lo3 in line with a biomass increase resulting in ^{15}N dilution in AMF inoculated plants (Supplementary Figure 4). These data indicate that the higher uptake of N triggered by *R. irregularis* is more likely to occur after the vegetative stage.

It is well established that mycorrhizae play a pivotal role in the improvement of plant P nutrition and uptake (Choi *et al.*, 2018; Plassard *et al.*, 2019; Paries and Gutjahr, 2023). To

determine if the amount of N supplied to the plant and the presence of *R. irregularis* modify B73 and Lo3 phosphate content, total P content (TPC) was measured by the molybdate blue method. In inoculated plants, an increase in the TPC content was observed under HN conditions both in the grains and in the roots of Lo3, whereas for B73 it was in the shoots and in the roots under HN (Figure 2B-D-F). Together, these data indicate that N supply has a strong impact on *R. irregularis* mediated P nutrition and that this benefit depends on maize genotype.

Inoculation by *R. irregularis* mitigate the physiological impact of N-deficiency

Physio-agronomic phenotyping prompted us to determine if there were traits that could discriminate inoculated and non-inoculated plants. For this purpose, hierarchical clustering analysis (HCA) was performed using the physio-agronomic traits listed in Supplementary Table 3. The HCA presented in Figure 3 shows that the N supply, the genotype, and the symbiotic association had an impact on the monitored traits. All the LN plants were grouped in cluster A. Within cluster A, values for the traits related to N and P uptake including root P content and ^{15}N enrichment (R_Ppercent and R_15NEpercent respectively), aerial part P content, NUE and ^{15}N enrichment (AP_Ppercent, AP_NUE, AP_15NEpercent respectively), were higher. LN plants in cluster A were distant from the HN MN plants clustered in group B. In cluster B, genotypes were distributed into two subgroups, B1 and B2. Traits related to yield and biomass were grouped in cluster B irrespective of the inoculation status. Interestingly, in cluster A, traits related to N deficiency exhibited higher values in the control compared to the inoculated plants indicating that *R. irregularis* allowed plants to behave more similarly to group B plants, albeit still under N stress deficiency. These data show that *R. irregularis* inoculation can mitigate the impact of N limitation on physio-agronomic traits.

Marker genes for N uptake and assimilation are differentially regulated in response to AMF inoculation and N supply

The finding that several NUE traits, notably those related to NO_3^- uptake were modified by AMF treatment prompted us to investigate further which molecular components were involved. Before investigating in detail, the molecular mechanisms taking place in regard to on N supply we had to identify the time point of the interaction process at which symbiotic markers were expressed at their maximum. For this purpose, the expression levels of symbiotic marker genes were monitored at three stages (see materials and methods). Then, the level of transcripts for the plant genes *ZmAMT3.1*, *ZmPHT6.1* and *ZmNPF4.5* markers of the symbiotic association and representative of NH_4^+, phosphorus and NO_3^- transport respectively was quantified (Sawers *et al.*, 2017; Wang *et al.*, 2020; Xie *et al.*, 2022; Hui *et al.*, 2022). For the three genes, the levels of root transcripts were higher at VT+15 stage in both HN and LN conditions (Supplementary Figure 5). Fungal colonization was greater under HN compared to LN both in B73 and Lo3 (Supplementary Figure 5A). Hence, the VT+15 stage was selected for all subsequent experiments.

The expression of selected marker genes involved in direct N transport, P and N transport mediated by AMF was then monitored in roots following inoculation by the AMF and according to the level of N supply. By monitoring the level of *R. irregularis* constitutive transcript *RiLSU* we confirmed that high N input led to increased fungal biomass in roots (Figure 4B). The expression level of the four well known symbiotic markers mentioned previously, *ZmPHT1.6*, *ZmNPF4.5*, *ZmHA1*, a proton pump, and *ZmAMT3.1* (Wang *et al.*, 2014, 2020; Sawers *et al.*, 2017; Xie *et al.*, 2022; Hui *et al.*, 2022), is up-regulated in response to the fungus in both genotypes and under all N supply conditions. It is interesting to notice that the higher the N nutrition level, the higher the expression of these markers (Figure 4A). To know more about direct N transport and N assimilation genes in those conditions, we investigated expression levels of two maker genes of N starvation stress *(ZmNRT2.1a, and ZmNRT2.2)* encoding high affinity transporters, known to be upregulated under N deficiency (Krapp *et al.*, 2014; Wang *et al.*, 2018; Dechorgnat *et al.*, 2019; Hirel and Krapp, 2020) (Figure 4A). As expected, the level of N supply had a drastic effect in both

maize genotypes on transcripts levels for the nitrate transporters *ZmNRT2.1a, ZmNRT2.2* which were more highly expressed in LN plants compared to MN and HN plants. These data indicate that the presence of the fungus mimics an additional N supply.

Leaf and root transcriptome reprogramming in response to *R. irregularis* colonization integrates a genotype and N-availability effects

To further characterize the biological processes involved in maize response to *R. irregularis* colonization as a function of N fertilization, a whole genome transcriptomic approach was conducted in leaves and roots of plants grown under HN and LN conditions. First, we defined the differentially expressed genes (DEGs) as those exhibiting a fold change of the transcript levels in inoculated plants compared to non-inoculated plants that was higher than 1.5 or lower than -1.5 ($p<0.05$). It is important to note that RNAs used for the transcriptomic approach were obtained from the plants that were phenotyped at the end of their life cycle for physio-agronomical traits. Indeed, root harvesting for molecular studies was not destructive, allowing plants to complete their life cycle.

Details for the numbers of DEGs depending on organ, N nutrition level and genotype are shown in Supplementary Figure 6. First, we focused on the DEGs in roots and in leaves irrespective of the genotype and irrespective of the level of N fertilization. In leaves, only 2 genes were up-regulated and only 2 genes were down regulated, whereas in roots many more genes were differentially expressed in all conditions in response to the fungus. The two genes up-regulated in all conditions in leaves encode a H(+)-exporting diphosphatase (Zm00001d015569) involved in vacuolar ion transport and a histidine-containing phosphotransferase protein 4 (Zm00001d043505) involved in signalling. The two down-regulated genes encode a Mannan endo-1,4-beta-mannosidase (Zm00001d010039) involved in cell wall remodelling and a Nuclear transcription factor Y subunit (NF-Y) (Zm00001d006835).

When considering root DEG genes irrespective of the genotype or N supply, there was an increase in the expression level of 345 genes whereas a decease was observed for 59 genes (Supplementary Figure 6). GO enrichment analysis revealed that for those common up-regulated genes in roots, the biological processes overrepresented were those related to proteolysis inhibition, lipid metabolism, ethylene response and membrane transport. The common down regulated genes were represented by five main functional categories including cell wall biogenesis, metal homeostasis, phosphate transport, stress responses and lipid metabolism (Figure 5).

To gain insight into the specific mechanisms taking place in each line (B73 and Lo3) upon symbiotic association as a function of N nutrition, enriched GO functions in DEG under LN or HN in each organ were determined. In B73 roots under LN, main overrepresented categories of up-regulated transcripts are related to plant immunity represented by hormone signaling and phenylpropanoid pathway, cell wall remodeling and nucleotide metabolism, while the main down-regulated categories were enriched in post translational modifications such as histone de-ubiquitination. In B73 roots under HN, the main overrepresented categories in up-regulated genes are related to defense, signaling, glycolysis, lipid metabolism and cellular trafficking while the overrepresented categories in the down-regulated genes are related to sugar and steroid metabolism and cell division.

In inoculated Lo3 roots under LN, stress responses, amino acid biosynthesis and autophagy are overrepresented in the up-regulated genes, while in the down-regulated genes, DNA and amino acid metabolism as well as cell wall remodeling are overrepresented. Under HN, *R. irregularis* inoculation of Lo3 triggers the up-regulation of root transcripts mainly related to photosynthesis, stress responses, DNA metabolism, water transport, amino-acid metabolism, root development and terpenoid biosynthesis. In roots of HN grown Lo3 plants, the main overrepresented categories of down-regulated genes belong to nitrate assimilation, oligopeptide transport and stress responses categories.

We performed the same data analysis in leaves (Figure 5). In response to *R. irregularis*, the B73 leaves main overrepresented categories of up-regulated transcripts under LN conditions are related to translation and auxin signaling, while the main down-regulated categories were enriched in symbiotic interactions, signaling. Under HN, in B73 leaves of inoculated plants, the main overrepresented categories in up-regulated genes are related to redox reactions, carbohydrate transport and defense while the main over-represented categories in the down-regulated genes are related to protein folding and response to inorganic substances.

In leaves of inoculated Lo3 plants, under LN, the main overrepresented categories in the up-regulated genes are photosynthesis, cell wall remodeling, cytoskeleton remodeling, stress response, signaling, while in the down-regulated genes, gamma-amino butyric acid (GABA) metabolism and pyrimidine biosynthesis are overrepresented. Under HN, *R. irregularis* inoculation of Lo3 plants triggers the up-regulation of leaf transcripts mainly related to amino acid catabolism, flavin-containing compounds related metabolism and organic acid transport as well as iron homeostasis, while down-regulated genes belong to lipid metabolism, pyrimidine metabolism, and stress response. Taken together, these data show that leaf and root transcriptomic responses to the AMF differ depending on maize genotype and N supply.

Leaf and root metabolomic profiles in response to *R. irregularis* are shaped by N nutrition

To further characterize the metabolic responses of the two maize lines to *R. irregularis* inoculation, a primary metabolome profiling was performed on the same leaf and root samples as those studied in the previous section. Metabolic profiles showed that plant organ and N supply had the strongest impact on leaf and root metabolite composition (Supplementary Figures 7A and B). AMF inoculation and maize genotype had globally weaker impacts on metabolite profiles (Figures 6 A and B and supplementary Figure 7C and D). In leaf samples 132 water soluble metabolites were detected of which 103 were significantly different in at least on condition after ANOVA statistical analysis ($P < 0.05$) followed by a Bonferroni post-hoc test and correction. In roots, there were 120 water-soluble

metabolites of which 117 were found to be significantly different in at least one condition. The identity of metabolites can be found on the interactive heatmap Supplementary interactive File 1.

In roots, fungal inoculation triggered accumulation of lipids such as trans-13-octadecenoic acid and palmitoleic in both lines Supplementary Figure 8. The accumulation of these two lipids was much higher under HN than under LN. We observed that in inoculated roots, there was a global decrease in sucrose, glucose and fructose levels in roots of Lo3 under LN. Several metabolites linked to N metabolism were differentially accumulated in inoculated roots. For example, Glu, Arg, citrulline, Asn and β-Ala levels were increased in response to *R. irregulari*s in roots under HN. Glutamine levels remained unchanged in inoculated roots. Some metabolites related to immunity were accumulated differentially in response to the fungus. For instance, shikimic acid was accumulated in LN roots of inoculated B73 plants and trehalose was accumulated in HN inoculated roots of both lines compared to controls.

In leaves, lipids and soluble sugars (glucose and fructose) did not show differential accumulation in response to the fungus. Sucrose, however, showed a significant decrease only for HN and this in both lines (Supplementary Figure 9). Gln and Asn accumulated in Lo3 leaves under HN in response to *R. irregularis*. Xylulose accumulated in Lo3 R LN leaves.

To identify metabolites representative of the plant response to *R. irregularis* under each growth condition, metabolites for which abundance is significantly correlated with specific treatment conditions were identified by using a variable selection approach in a multivariate linear model conducted with the MultiVarSel approach (see materials and methods, Figure 6 C and D). For example, we found that under LN, xylulose was accumulated in leaves of Lo3 inoculated plants (Figure 6C). In roots, benzoic acid was accumulated in inoculated B73 roots of plants grown under LN (Figure 6D). Palmitoleic acid is accumulated to a lower extent in Lo3 HN control conditions compared to all the other conditions. These data indicate that specific metabolites are accumulated depending on the plant genotype and the N supply in response to *R. irregularis*.

Multi-organ metabolic modelling reveals key metabolic processes triggered by *R. irregularis* allowing maize to mitigate N limitation stress

To identify key metabolic reactions involved in yield and biomass reshaping in response to *R. irregularis* symbiosis, we integrated the transcriptomic data in a recently reconstructed multi-organ genome scale modelling (GSM) named *i*ZMA6517 (Chowdhury *et al.*, 2023), This model was built for the B73 maize genotype using the transcriptomic data integration algorithm, EXTREAM (Chowdhury *et al.*, 2023). This was followed by a metabolic bottleneck analysis (MBA) to pinpoint metabolic bottlenecks for biomass production. The B73 leaf and root transcriptomic data were used as input to EXTREAM to contextualized *i*ZMA6517. The modelling predicted that growth rates were higher under LN in response to *R. irregularis* inoculation compared to non-inoculated plants, which resulted in grain yield and biomass increase while under HN, a negative impact on maize growth rate was observed (Figure 7A). Strikingly, these data are in agreement with the observed yield and biomass experimental data in Figure 1, confirming the accurate phenotypic prediction of the *i*ZMA6517. This result prompted us to determine the metabolic processes that could explain the improved yield under LN B73 plants in response to *R. irregularis* inoculation by identifying the potential metabolic bottlenecks relieved by the AMF under limiting N. For this purpose, we compared the bottlenecks identified in LN control plants to the bottlenecks identified in inoculated LN plants (Figure 7B; Table 1). Four metabolic bottlenecks relieved by *R. irregularis* inoculation were identified : photosynthesis, purine and pyrimidine metabolism, aromatic acid metabolism; and folate metabolism (Figure 7B, Table 1). Interestingly 13 new bottlenecks were emerged following *R. irregularis* inoculation. These new bottlenecks are involved in the metabolism of nicotinate, nicotinamide, purine, aromatic amino acids, Calvin cycle and glycolysis, On the other hand, we found that in HN plants, four metabolic bottlenecks that were present in LN control plants were relieved. Three of them were common with those relieved by *R. irregularis* (photosynthesis, purine and pyrimidine metabolism, aromatic acid metabolism), the fourth one is involved in ascorbate and aldarate metabolism. The HN

treatment created 14 new metabolic bottlenecks compared to LN control conditions. These new bottlenecks are involved in glycolysis, TCA cycle, Calvin cycle, metabolism of alanine, aspartate, glutamate, pyrimidine, purine, fructose, mannose, aromatic amino acids. These data indicate that different metabolic processes are modulated by N supply and *R. irregularis* inoculation. The most interesting result is the fact that photosynthesis, pyrimidine metabolism, aromatic amino acid biosynthesis are 3 processes likely to play key roles on *R. irregularis* mediated N nutrition in maize.

Transcriptome of *R. irregularis* in inoculated maize roots is driven by N availability

To gain insight into the metabolic cross talk between *R. irregularis* and maize, we investigated the biological processes taking place in the fungal partner according to the N supply conditions. For this purpose, we determined the fungal genes displaying a higher expression in LN roots compared to HN roots and vice versa. This selection was performed for B73 and Lo3 separately. The Venn diagrams in Figure 8A and 8B show that under LN, 1251 fungal genes were up-regulated in Lo3 while they were 1247 in B73, including 548 transcripts up-regulated in both maize lines. In HN roots, 1596 fungal transcripts were up-regulated in Lo3 and 1359 were up-regulated in B73 roots including 609 genes up-regulated in both maize lines. In both maize lines, the functional categories overrepresented in *R. irregularis* DEG were similar in each N nutrition condition Figure 8C. However, an important remodelling in *R. irregularis* overrepresented DEG functional categories in response to N supply was observed. For example, fungal genes up-regulated under LN were involved in nuclear structures, vesicular trafficking, translation and transcription, whereas those up-regulated under HN had a role in metabolic activity of primary and secondary metabolism, in particular nucleotide and lipid metabolism. Only few maize line-specific functional categories could be observed. For instance, defence mechanisms was a functional category of *R. irregularis* DEGs specifically expressed in Lo3. These data show that the fungal transcriptome is strongly affected by the nutritional N status of the host and the soil. Among the DEG functional categories, several genes were involved in amino acid and nucleotide

metabolism and transport as well as in inorganic transport. We focused on the expression profiles of nucleotide and amino acid metabolism genes and transporter genes as well as phosphate and ammonium acid transport genes. Supplementary Table 7 shows the expression pattern of these fungal genes. Interestingly, fungal ammonia transporters are more highly expressed under LN than under HN. We did not find any fungal nitrate transporter genes in the differentially expressed AMF genes. The fungal amino acid biosynthetic genes up-regulated are mainly involved in asparagine, arginine, glutamine, glutamate and serine pathways. Several fungal amino acid transporter genes were found to be up-regulated either in LN or HN roots. The fungal nucleotide biosynthesis genes up-regulated in HN roots are related to pyrimidine de novo biosynthesis or salvage pathways.

Discussion

To better understand the biological and genetic basis of how AMF improve maize N nutrition, we investigated the physiological and molecular responses of different maize genotypes when they are inoculated with the AMF *R. irregularis* under different N supply conditions. In our study, the first interesting result was to find an increase in kernel yield in the two maize lines B73 and Lo3 inoculated with *R. irregularis* when N nutrition is reduced. We showed that a symbiotic association with *R. irregularis* was able to compensate for decreased maize plant performance when N fertilization is reduced. In the literature, depending on both the N supply level and the form of N supplied, different effects on yield and/or biomass production have been reported, including an increase, no effect, or a reduction in productivity when the plant develops a symbiotic association with an AMF (Ingraffia *et al.*, 2020; Quiroga *et al.*, 2020; Yooyongwech *et al.*, 2022). In the present investigation, we estimated that kernel yield can be maintained with a 2- to 5-fold reduction in N input when two maize lines were inoculated with *R. irregularis*. Such a beneficial impact was previously observed for maize plant biomass production under low N fertilizer inputs (Quiroga *et al.*, 2020). One can, therefore, conclude that the positive impact of AMF on plant performance can be variable depending on the AMF and the host genotype as well as the level and type of available N source (Verzeaux *et al.*, 2017; Ingraffia *et al.*, 2020; Xie *et al.*, 2022).

Our transcriptome study allowed us to provide an overview of biological processes putatively involved during the establishment of a symbiotic association between the AMF *R. irregularis* and maize. In the leaves of inoculated plants, four maize genes were found to be differentially expressed irrespective of the N-feeding conditions and the genotype (Zm00001d015569, Zm00001d043505, Zm00001d010039, Zm00001d006835). Although these four genes did not allow us to identify a core biological process occurring in inoculated plants, their function was representative and biologically relevant to an interaction with an AMF such as biomass production (Zm00001d015569) (Menadue *et al.*, 2021), cytokinin signaling (Zm00001d043505) (Yonekura-Sakakibara *et al.*, 2004), cell wall remodeling

(Zm00001d010039), nitrate transport and flowering (Zm00001d006835) (Su *et al.*, 2018; Cheng *et al.*, 2021).

Whatever the level of N fertilization or the maize lines, the core DEGs that were either up or down-regulated in roots were enriched in transcripts encoding proteins involved in a variety of biological functions : defense, hormone signaling (especially jasmonate and cytokinin), N and C metabolism, cell wall and chromatin remodeling, proteolysis inhibition, metal homeostasis, phenylpropanoid and lipid metabolism. Similar results were previously obtained in several other model and crop species, indicating that most of these biological functions are shared when plant develop symbiotic associations with AMFs (Fiorilli *et al.*, 2009; Gallou *et al.*, 2012; Schaarschmidt *et al.*, 2013; Meng *et al.*, 2015; Handa *et al.*, 2015; Vangelisti *et al.*, 2018; Kaur and Suseela, 2020; Wang *et al.*, 2020; Hui *et al.*, 2022). In particular, the most highly up-regulated genes in roots of B73 and Lo3 under both N nutrition conditions in response to *R. irregularis* inoculation are encoding peptidases, peptidase inhibitors, chitinases and senescence genes (Supplementary Table 10a and b). Interestingly, autophagy genes are overrepresented in Lo3 genes up-regulated in roots under LN following inoculation with *R. irregularis* (Supplementary Table 9, Figure 5). These data suggest that important proteolysis processes are taking place in in inoculated roots that may involve autophagy especially in the Lo3 maize line. Autophagy is a process known to recycle N during senescence, and is known to provide N assimilates necessary for maize kernel filling (Li *et al.*, 2015; Masclaux-Daubresse *et al.*, 2017).

Changes in the level of expression of genes involved in sugar, amino acid, and lipid metabolism were confirmed by metabolomics analyses (Supplementary Figure 8 and 9). Under HN, the amounts of root soluble carbohydrates sucrose, fructose, and glucose were lower in inoculated plants compared to controls, which is consistent with the export of C-containing molecules to the fungus. As this did not occur under LN, one can hypothesize that the roots and/or the fungus do not constitute an important sink for C or that the plant limits fungal proliferation under N-limiting conditions. Under LN, genes involved in the control of

plant immunity were up-regulated in roots of inoculated plants, especially in line B73, which is consistent with the accumulation of shikimic acid (Supplementary Figure 8). Both transcriptomic data and metabolomics data show modifications in lipid metabolism and the accumulation of lipids in roots. In roots, when N fertilization was not limiting, we observed an accumulation of two lipids: trans-13-octadecenoic acid and palmitoleic acid (Supplementary Figure 8). Lipid accumulation in roots colonized by AMFs was already observed (Keymer *et al.*, 2017; MacLean *et al.*, 2017), notably in *R. irregularis*, to which their reduction and transfer from the host to the fungus is considered to be a way of fueling the symbiotic fungus with a carbon source other than sugars (Keymer *et al.*, 2017; MacLean *et al.*, 2017). In the present study, lipid accumulation occurred only under HN, which is consistent with the fact that due to higher photosynthetic activity, as revealed by the accumulation of soluble carbohydrates, the plant is able to synthesize more fatty acids to feed the fungus. In inoculated plants, arginine (Arg), known to be a key molecule involved in the transfer of N from the fungus to the plant (Chen *et al.*, 2018*a*; Kaur and Suseela, 2020; Dellagi *et al.*, 2020; Xie *et al.*, 2022), accumulates under HN conditions not only in the roots of line B73 HN but also in the leaves.

Unexpectedly, another process that appears to be playing a crucial role in AMF symbiosis is pyrimidine biosynthesis. Our transcriptomic analysis demonstrates that, regardless of nitrogen feeding conditions, pyrimidine biosynthesis processes are consistently downregulated in leaves of inoculated plants (Figure 5). Furthermore, under low nitrogen (LN) conditions, several key genes encoding enzymes involved in nucleotide metabolism, including carbamoyl-phosphate synthase (Witte and Herde, 2020*b*), are downregulated in both leaves and roots (Supplementary Table 8). For example, maize carbamoyl-phosphate synthase genes *Zm00001d044250 Zm00001d011192* are downregulated in B73 roots when inoculated with *R. irregularis* under LN conditions (Supplementary Table 8). A critical gene in this context is *Zm00001d023833*, encoding a putative nucleoside diphosphate kinase (NDPK), which participates in pyrimidine and purine nucleotide salvage (Witte and Herde,

2020*a*). This enzyme was identified as a metabolic bottleneck relieved by AMF inoculation (Figure 7). More precisely, the reactions relieved by *R. irregularis* inoculation corresponds to those indicated in Figure 7. In non-inoculated maize plants under LN, this maize *NDPK* gene is up-regulated in leaves compared to HN suggesting that pyrimidine salvage is activated under LN to help plants cope with N Limitation (Supplementary Table 8). On the contrary, in the symbiotic association, *NDPK* gene expression remains unaltered compared to uninoculated LN, suggesting the absence of constraints on this enzymatic reaction in symbiotic plants (Supplementary Table 8). The level of β-Ala, a known product of purine degradation drops in inoculated LN and HN roots suggesting that *R. irregularis* inoculation represses the degradation of nucleotides.

In line with these data, fungal transcriptomic analysis by RNAseq shows that pyrimidine and ureide metabolism play a crucial role in the symbiosis with regard to N nutrition. The fungal metabolism appears to differ depending on N supply. The integration of maize and fungal RNAseq and metabolome analyses has allowed us to construct a simplified model depicting the various biological events occurring in the symbiotic association (Figure 9). Under LN, fungal argininosuccinate lyase, carbamoyl-phosphate synthase and arginase genes are upregulated, potentially leading to urea accumulation. However, urea level drops in LN inoculated roots a fact that is consistent with higher expression of *R. irregularis* urease under LN. It is thus likely that under LN, the major way the fungus provides plant with N is based on its urea cycle followed by urea conversation into ammonium which is then transferred to the plant.

Under HN, several amino acids accumulate in response to fungal inoculation in roots (Gln, Glu, Asn, Arg, Citr, Orn). Fungal pyrimidine de novo biosynthetic genes and the pyrimidine salvage pathway are upregulated in HN roots. This suggests that under HN, the fungus activates the metabolism of nucleotide monophosphate biosynthesis that may then be transferred to the plant. The transfer of nucleotides from the fungus to the plant could also

take place under LN but to a lower extent because metabolic modeling identified the NDPK enzyme as being the metabolic bottleneck relived by *R. irregularis* inoculation under LN.

On the other hand, allantoin accumulates exclusively in HN roots and its level remains unaffected by inoculation. This metabolite can be converted into allantoic acid, which may be released into the apoplast (Tegeder, 2014). A fungal allantoicase is upregulated in HN roots, indicating possible conversion of allantoic acid into urea under HN conditions. This transfer of ureides is akin to the process observed in symbiotic associations between tropical legumes and Rhizobia species (Tegeder, 2014). Previous studies have also identified upregulation of genes involved in allantoin synthesis in roots of AMF-inoculated plants (Nanjareddy *et al.*, 2017). Consequently, it is plausible that ureide transfer mirrors that occurring in legume nodules.

Fungal arbuscules are known to undergo controlled senescence (Choi *et al.*, 2018; Paries and Gutjahr, 2023), our data suggest that autophagy is upregulated in maize roots, with higher expression in Lo3 LN roots (Supplementary Table 9). Autophagy likely contributes to the degradation of fungal cellular products, potentially releasing nucleosides. The fungal nucleotide salvage process can then recycle nucleosides that may repress de novo plant pyrimidine biosynthesis pathways (Tegeder, 2014; Witte and Herde, 2020*b*). This implies that AMF likely supplies the host plant with nucleotides and nucleosides, potentially pyrimidines, to circumvent the deficiency in NDPK activity, thereby alleviating the associated metabolic bottleneck. This observation is consistent with the known role of NDPK in plant survival with respect to pyrimidine salvage (Tegeder, 2014; Witte and Herde, 2020*a*). It is noteworthy that pyrimidine biosynthesis can be an essential process for plant N management (Zrenner *et al.*, 2006; Fernie *et al.*, 2020).

Pyrimidine metabolism holds significance not only in crop performance but also in nitrogen use efficiency (NUE) (Tegeder, 2014; Lee *et al.*, 2018; Melino *et al.*, 2022). Recent findings demonstrate a correlation between maize leaf nitrogen accumulation and NDPK protein levels (Urrutia *et al.*, 2023), further supporting the hypothesis that *R. irregularis* stimulates the

reprogramming of plant pyrimidine metabolism to enhance maize performance under nitrogen-limiting conditions.

In conclusion, we propose that inoculating maize with *R. irregularis* offers a promising strategy to significantly reduce nitrogen fertilizer usage while maintaining maize kernel yield. Our findings highlight a metabolic interplay between the host and AMF, with pyrimidine and ureide metabolism serving as key players in this interaction (BARROSO *et al.*, 1988; Thakur and Garg, 2023). Furthermore, the observed differences in how our two studied maize lines embrace different strategies to benefit from the fungus illustrate the importance of leveraging maize's extensive genetic diversity for a comprehensive understanding of this symbiotic interaction (Schmidt *et al.*, 2016; Sawers *et al.*, 2018*b*; Liu *et al.*, 2020).

Data Availability

RNAseq project is deposited (Gene Expression Omnibus,Edgard R. et al. 2002): https://www.ncbi.nlm.nih.gov/geo/query/acc.cgi?acc=GSE235654 ; accession no. GSE235654. All steps of the experiment, from growth conditions to bioinformatic analyses, were detailed in CATdb (Gagnot *et al.*, 2008): http://tools.ips2.u-psud.fr.fr/CATdb/; Project: NGS2021_19_Rhizophagus according to the MINSEQE 'minimum information about a high throughput sequencing experiment'.

Acknowledgments:

BD acknowledges Université Paris Saclay for PhD fellowship. AD acknowledges the benefits received from France 2030 program (Saclay Plant Sciences, reference n° ANR-17-EUR-0007, EUR SPS-GSR integrated into France 2030 (reference n° ANR-11-IDEX-0003-02), INRAE Grant IB BAP 2021 MYCORN, and IJPB's Plant Observatory technological platforms. RS gratefully acknowledges funding support from National Science Foundation (NSF) CAREER grant (1943310) and Nebraska Collaboration Initiative Grant (21-1106-6011). We thank Michel Lebrusq, Lilan Diahuron, Patrick Grillot, and Christian Jeudy for taking care of the plants in the greenhouse. We thank the POPS platform for the RNAseq experiment and data. We also thank Etienne Delannoy from POPS platform for fruitful discussions. We are grateful to Cyril Bauland and Carine Palaffre from the INRAE for providing seeds from the Centre de Ressources Biologiques of Saint Martin de Hinx (France). We acknowledge Pr. Mario MOTTO from ISC, Bergamo (Italy) for providing Lo3 seeds.

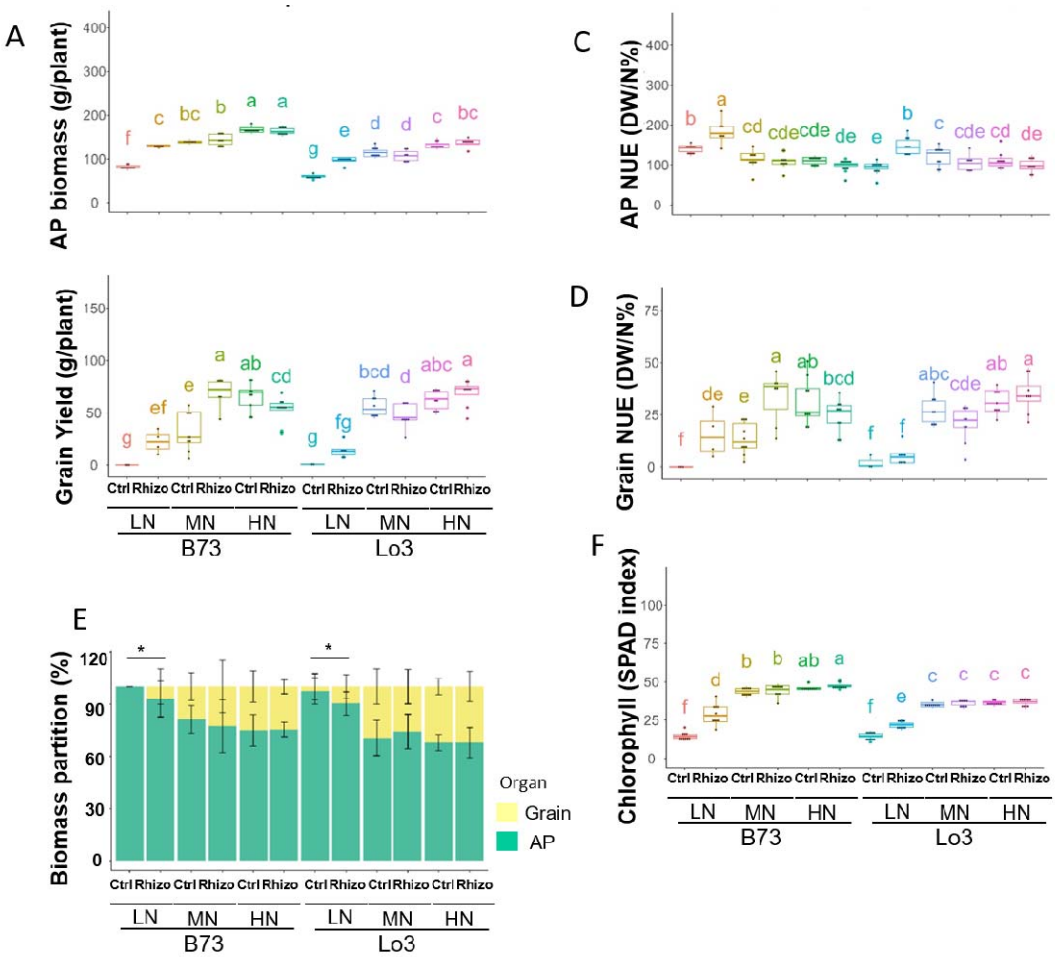

Figure 1: Impact of N supply on maize responses to *R. irregularis* for biomass and N content shows more pronounced beneficial AMF effects under LN. Plants were grown and harvested as indicated in materials and methods under low nitrate (LN, 1mM NO_3^-), moderate nitrate (MN, 5mM NO_3^-) or high nitrate (HN, 10mM NO_3^-). **A** and, **B** : grain yield and aerial part (AP) biomass of indicated samples. **C,D** : Nitrogen Use Efficiency (NUE) in grains and in AP. **E**: Biomass partitioning. **F**: Average chlorophyll content measured as SPAD index on the leaves number 4,5 and 6 over 5 weeks after sowing. Ctrl: Mock non inoculated control, Rhizo: inoculated with *R. irregularis,* AP: Biomass of Aerial Parts. N=7 to 10 plants. Different letters indicate significantly different averages for the considered trait by ANOVA. Asterisk indicates significant difference between control and inoculated plants t-test (p<0.05).

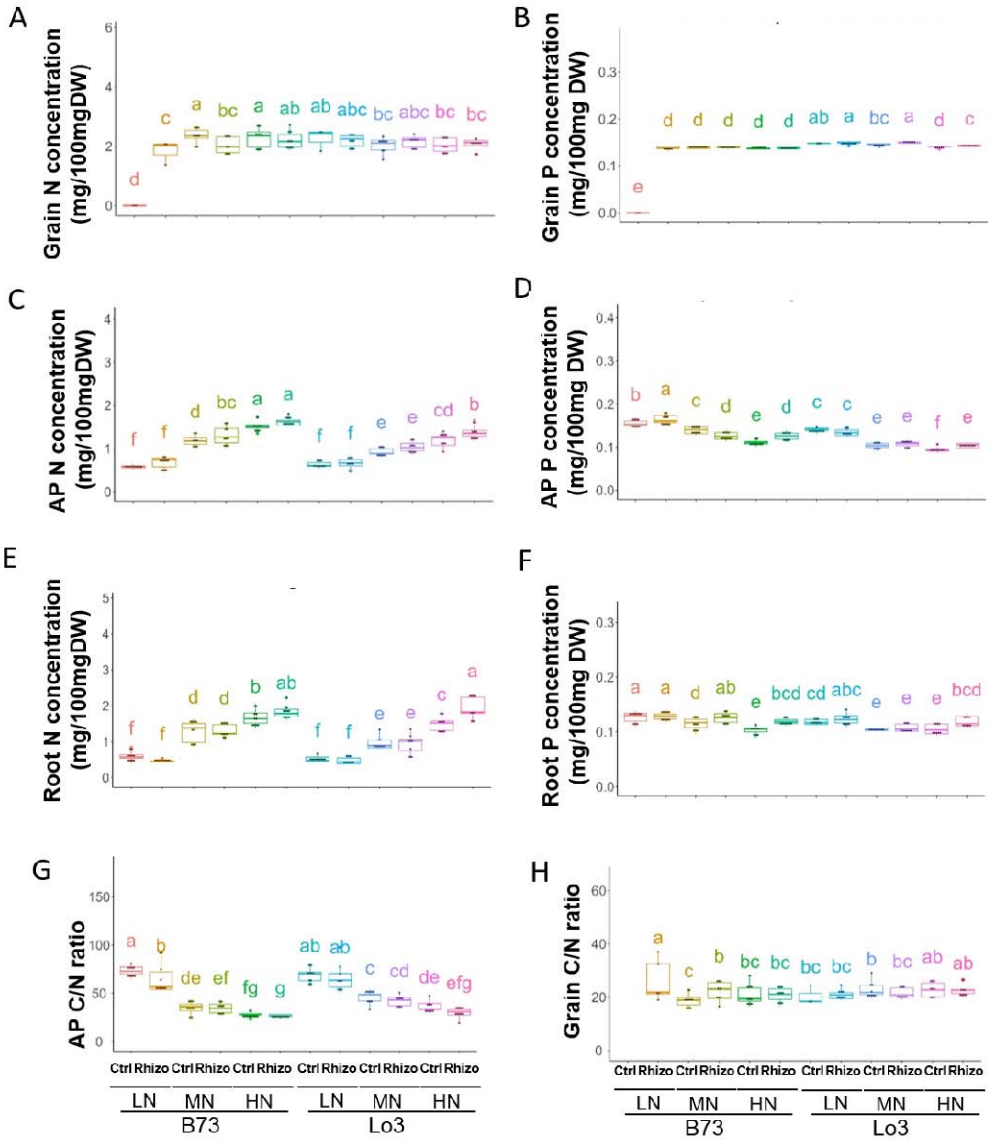

Figure 2: Impact of N supply on maize responsiveness to *R. irregularis* for P and N content and C/N ratio highlights poor impact of AM symbiosis on these traits. Plants were grown and harvested in 2020 as indicated in materials and methods under low nitrate (LN, 1mM NO_3^-), moderate nitrate (MN, 5mM NO_3^-) or high nitrate (HN, 10mM NO_3^-). **A** to **F** : N and P content of grains, aerial parts (AP) and roots. **G** and **H** : C/N ratios in AP and grains. Ctrl: Mock non inoculated control, Rhizo: inoculated with *R. irregularis* N=7-10 plants for grains and AP. N=5 for roots. Different letters indicate significantly different averages for the considered trait by ANOVA.

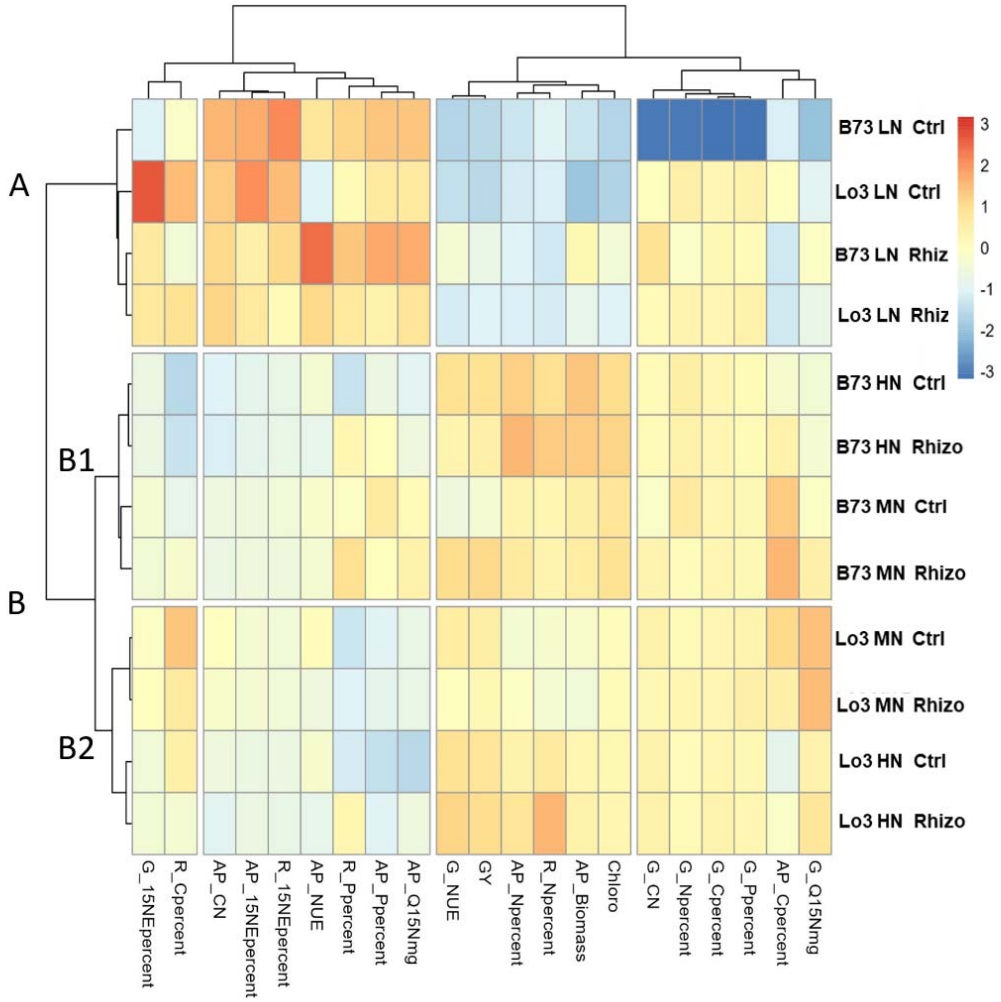

Figure 3: Heatmap of physio-agronomical traits in different organs shows that *R. irregularis* inoculation of LN plants improves their performances. Plants were grown and harvested in 2020 as indicated in materials and methods under low nitrate (LN, 1mM NO_3^-), moderate nitrate (MN, 5mM NO_3^-) or high nitrate (HN, 10mM NO_3^-). Standardized levels of quantified physio-agronomic traits of B73 and Lo3 lines under LN, MN or HN inoculated or not with *R. irregularis* are shown. The two HCA were performed to group the samples and the physio-agronomic traits according to their average values following Ward method of clustering. At the left of the HCA, the vertical bar represents the groups of samples. Indicated traits are measured in Aerial parts (AP), roots (R) or grains (G). Group A corresponded to plants grown under LN, Group B corresponded to plants grown under MN or HN. The B group was subdivided into two subgroups: B1 and B2 corresponded respectively to B73 and Lo3 plants. Ctrl: Mock non inoculated control, Rhizo: inoculated with *R. irregularis.* Three organs were considered: Aerial Parts (AP), Grains (G) and Roots (G). Chloro: chlorophyll monitored by SPAD index. Cpercent: Percentage of C. Npercent: percentage of N. CN: C/N ratio. 15NEpercent: percentage of ^{15}N. P Percent: percentage of P. Q15Nmg: quantity of 15N in organ per plant. NUE: Nitrogen Use Efficiency. GY: Grain Yield per plant. The color scale indicates if the trait is higher (orange) or lower (blue) in the indicated conditions with respect to the others. Details for the formulas used to calculate these traits are indicated in Supplementary Table 3.

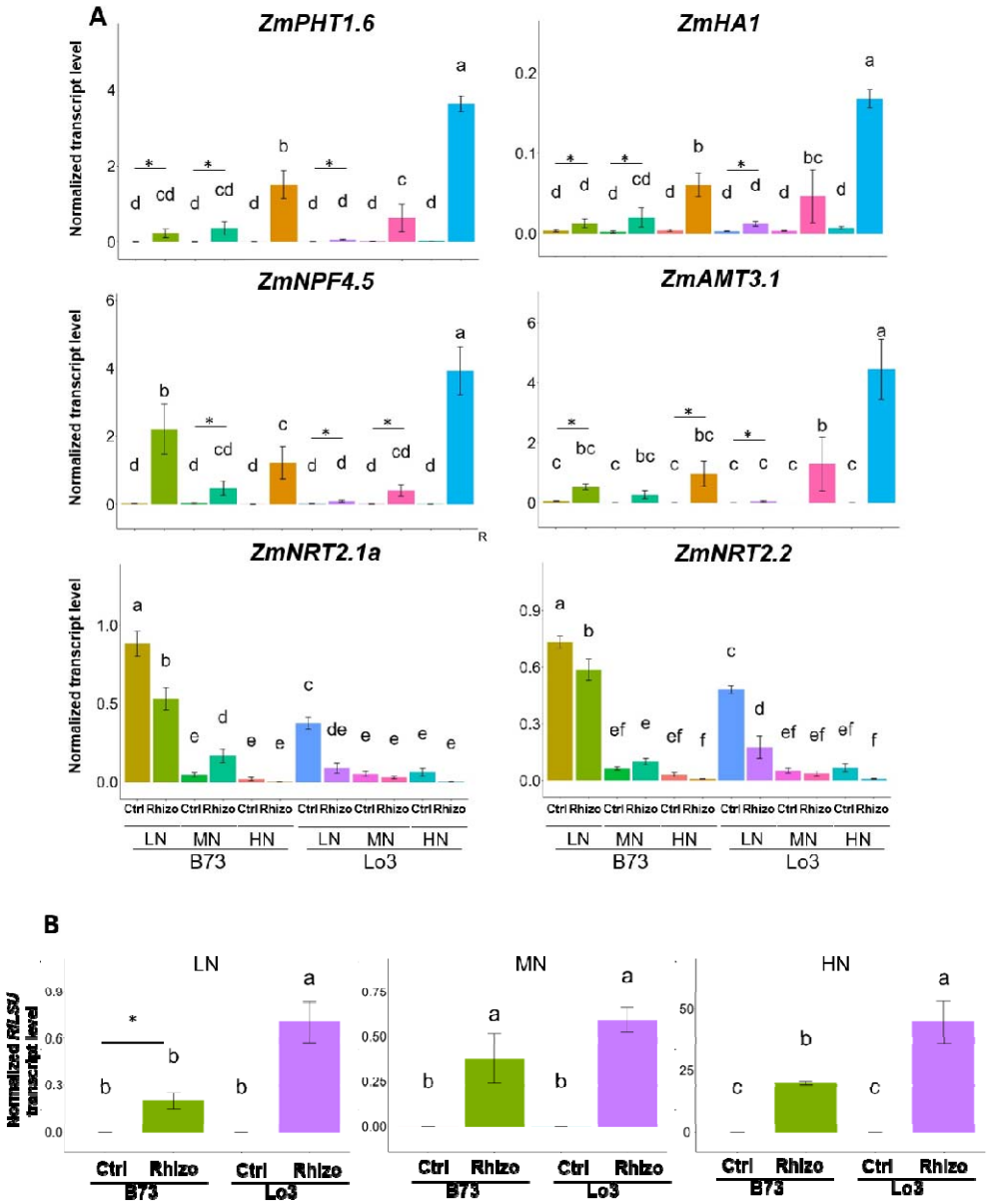

Figure 4: Impact of N supply on expression of genes involved in N and P transport in roots suggests that AM symbiosis alleviates N deficiency stress. Plants were grown and harvested in 2020 as indicated in materials and methods under low nitrate (LN, 1mM NO_3^-), moderate nitrate (MN, 5mM NO_3^-) or high nitrate (HN, 10mM NO_3^-). Roots were harvested at VT+15 stage. **A**: Normalized transcript levels of indicated genes monitored by qRT-PCR. **B:** Quantification of *R. irregularis* in roots by qRT-PCR amplification of the *RiLSU* constitutive fungal transcript. Ctrl: Mock non inoculated control, Rhizo: inoculated with *R. irregularis,* N=5. Different letters indicate significantly different gene expression levels as analyzed by ANOVA. Bars are standard errors. Asterisk indicates significant difference between mock and *R. irregularis*-inoculated plants by t-test (p<0.05).

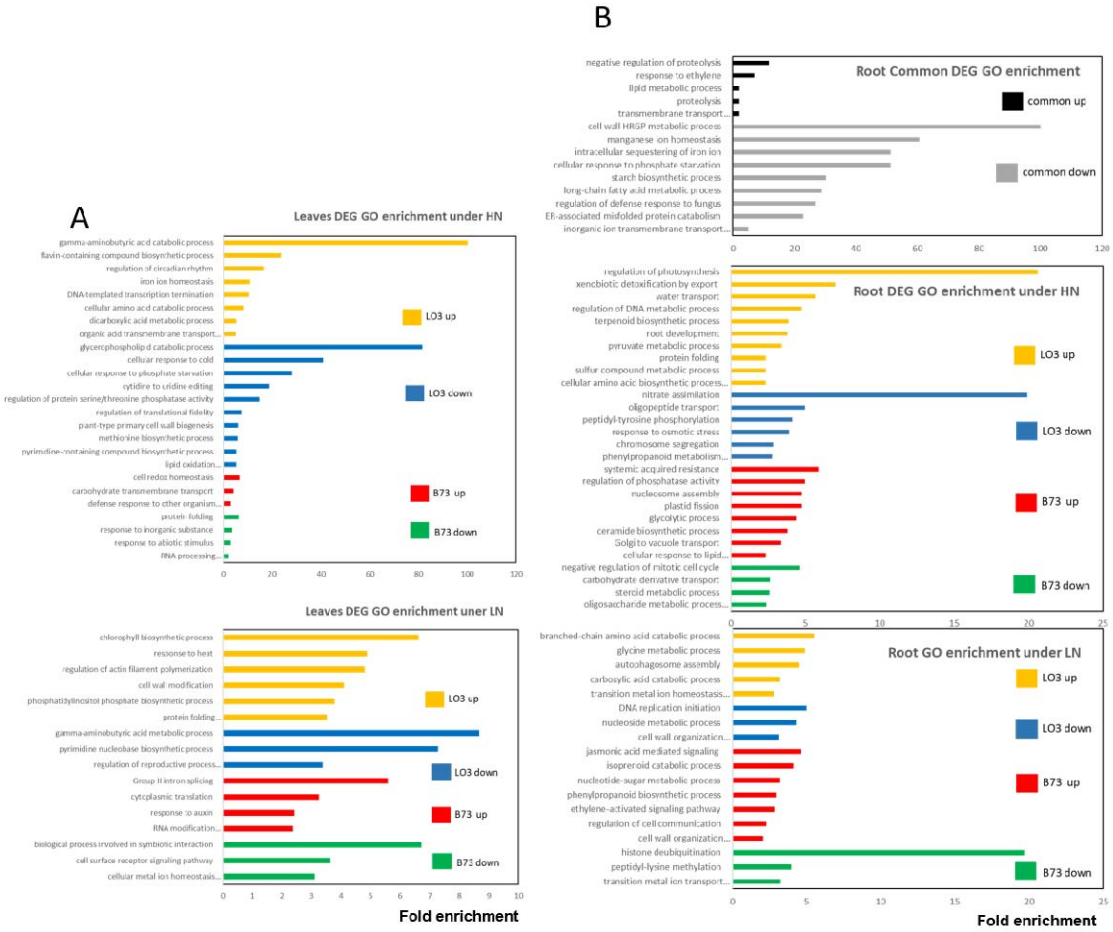

Figure 5 : Gene ontology of the enriched functional categories in the common DEGs. A: Leaf genes. **B**: Root genes. Common DEGs were selected so that they have the same pattern of regulation (up or down) in the different conditions with a fold change (FC) >1.5. FC represents the ration of expression of each gene in *R. Irregularis* inoculated tissues versus the mock control tissues. There were only 2 genes in the common DEGs in leaves thus, they were not included in the GO analyses. Each bar represents the fold enrichment in the indicated category obtained by https://pantherdb.org/. Only categories enriched more than 2 fold and displaying more than 2 genes are represented with *p*-value of enrichment < *0.05*.

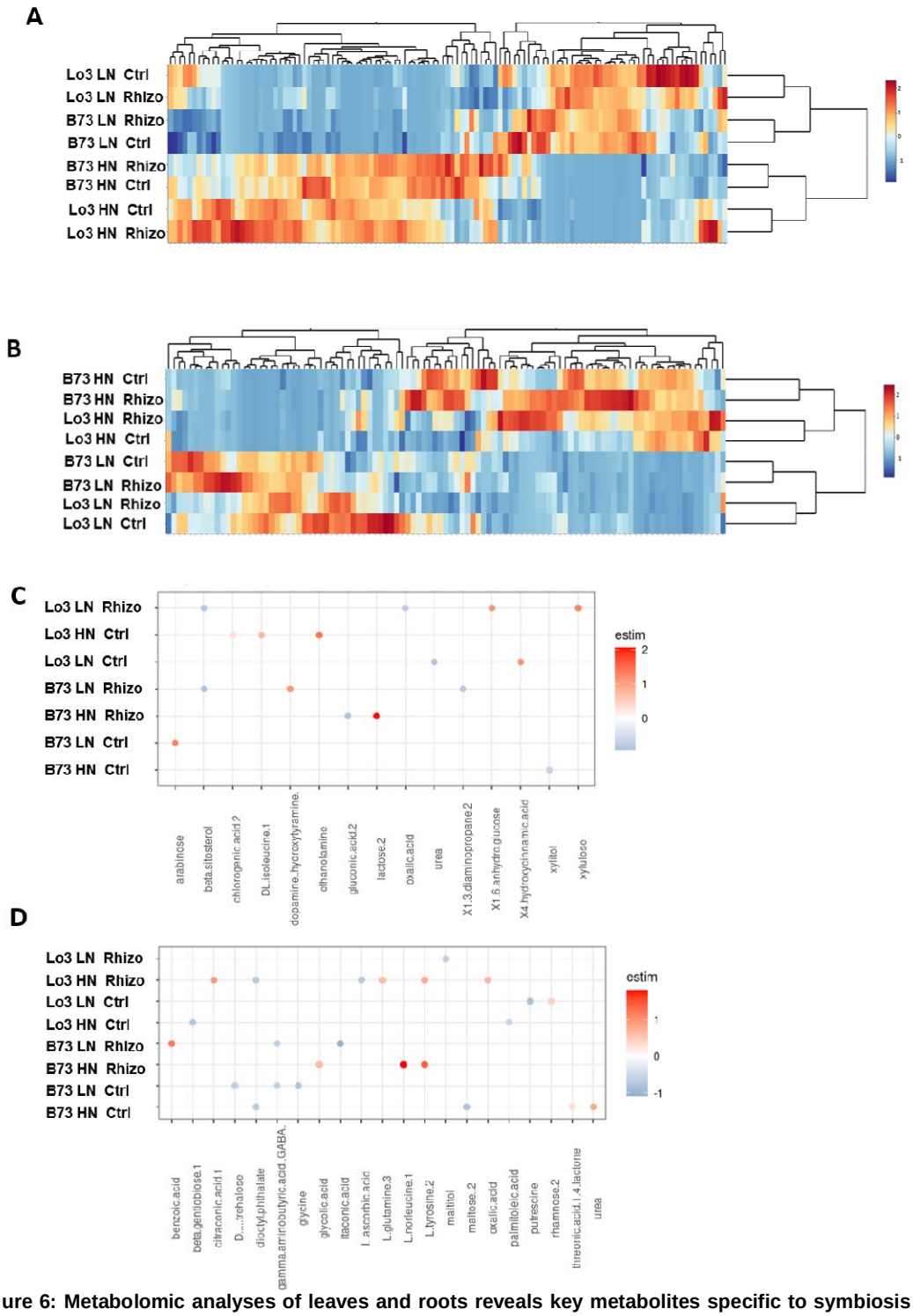

Figure 6: Metabolomic analyses of leaves and roots reveals key metabolites specific to symbiosis under LN or HN nutrition. Plants were grown and harvested in 2020 as indicated in materials and methods under low nitrate (LN, 1mM NO_3^-) or high nitrate (HN, 10mM NO_3^-). Leaves and roots were harvested at VT+15 stage. Ctrl: Mock non inoculated control, Rhizo: inoculated with *R. irregularis,* Metabolites were monitored by GS/MS. **A** and **B :** HCA heatmap showing metabolomic profiles of leaves and roots of inoculated or control plants under LN or HN in leaves and roots respectively. **C** and **D**: Analyses of metabolomics data conducted with the R package MultiVarSel with a threshold of 0.884 showing the metabolites on which the genotype, the N nutrition of the *R. irregularis* inoculation have an impact. Leaves, **C;** roots, **D.** The color scale indicates if the metabolites are accumulated (red) or down accumulated (blue) in the indicated conditions with respect to the others.

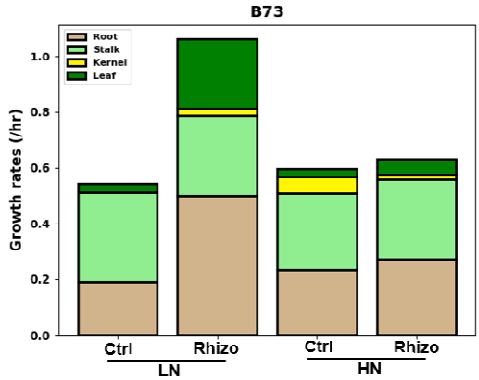

B

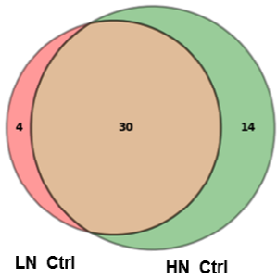

Reactions Debottelnecked by HN treatment	
R03817[M,t]	Photosynthesis light reactions
R00124[R,p]	Pyrimidine metabolism
R00692[R,p]	Phenylalanine, tyrosine, and tryptophan metabolism
R00095[R,x]	Ascorbate and aldarate metabolism

C

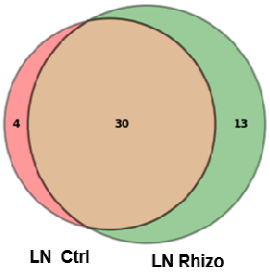

Reactions Debottelnecked by *R. irregularis* treatment	
R03817[M,t]	Photosynthesis light reactions
R00124[R,p]	Pyrimidine metabolism
R00692[R,p]	Phenylalanine, tyrosine, and tryptophan metabolism
R04241_mod[R,m]	Folate metabolism

D

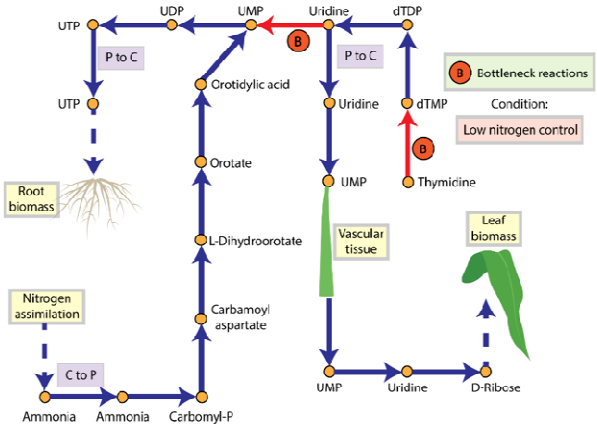

Figure 7: Genome based metabolic modeling reveals essential impact of AMF on pyrimidine metabolism. **A**: RNAseq data were used to predict different organ growth rates in the B73 maize line. Ctrl: Mock non inoculated control, Rhizo: inoculated with *R. irregularis,* EXTREAM algorithm predicted higher yield under LN in B73. **B** and **C**: Venn diagrams showing the metabolic bottlenecks under indicated conditions highlighting the debottlenecked reactions by uninoculated HN versus uninoculated LN (B) and by *R. irregularis* inoculation under LN vs uninoculated LN (C). **D**: Metabolic reactions in the pyrimidine pathway de-bottlenecked by *R. irregularis* inoculation and by HN treatment shown in **B** and **C**. P: Plastid compartment. C: Cytosolic compartment.

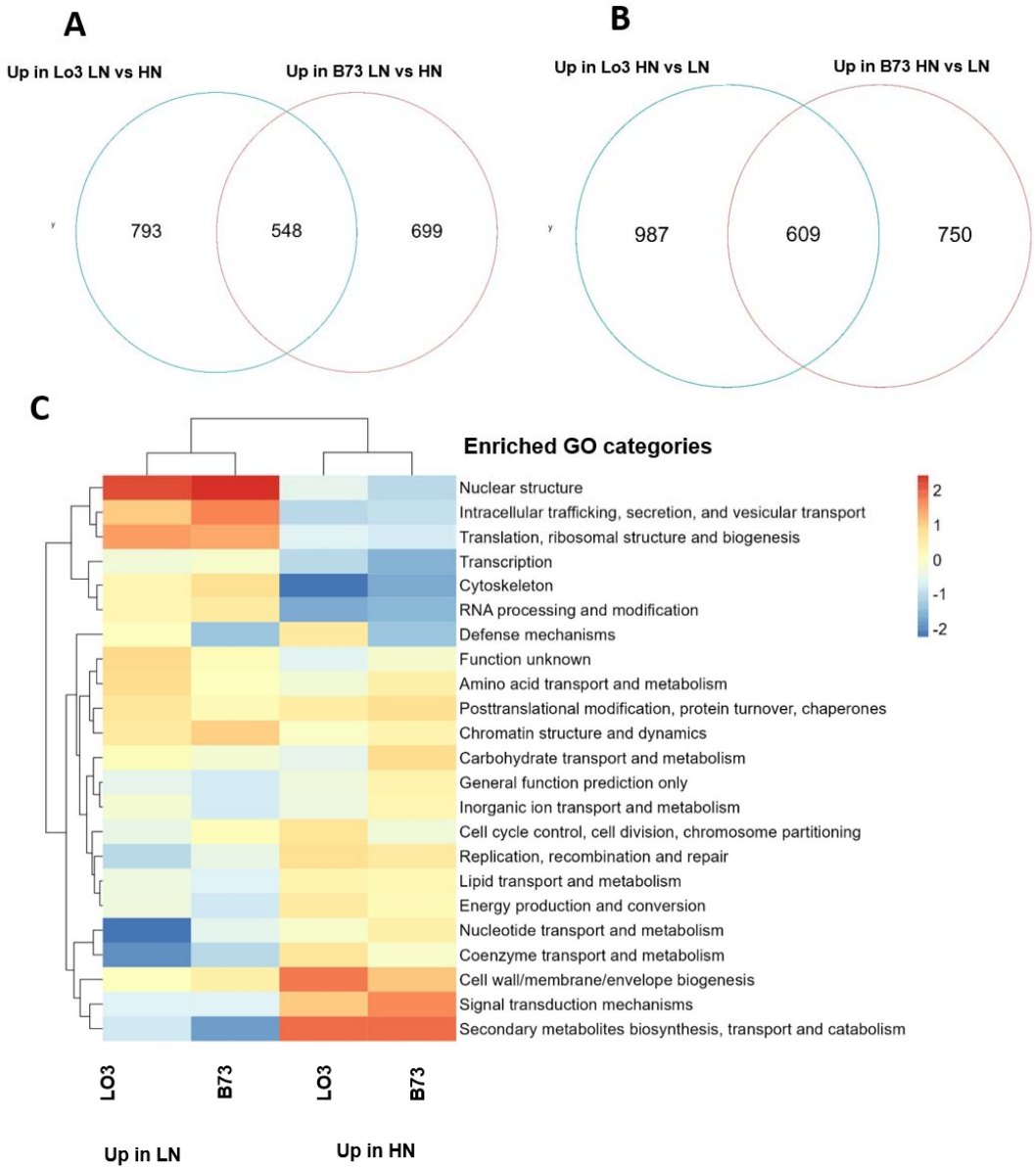

Figure 8 : *Rhizophagus irregularis* transcriptome in maize roots is shaped by N supply. Plants were grown and harvested as indicated in materials and methods under low nitrate (LN, 1mM NO_3^-) or high nitrate (HN, 10mM NO_3^-). Roots inoculated with *R. irregularis* were harvested at VT+15 as indicated in materials and methods. DEGs were selected so that they have a fold change (FC >1.5). **A** : Up in LN indicates *R. irregularis* genes that are more highly expressed in inoculated LN roots compared to inoculated HN roots. **B**: Up in HN indicates *R. irregularis* genes that are more highly expressed in HN compared to LN. **C**: Gene ontology of functional categories enrichment was based on KOG annotations of encoded *R. irregularis* proteins (see materials and methods). Each bar represents the functional category enriched in the given condition. p-value of enrichment was < 0.05; only categories enriched more than 2 fold and displaying more than 2 genes are represented and used to build the heatmap. The color scale indicates the over-representation or the down-representation in red and blue respectively.

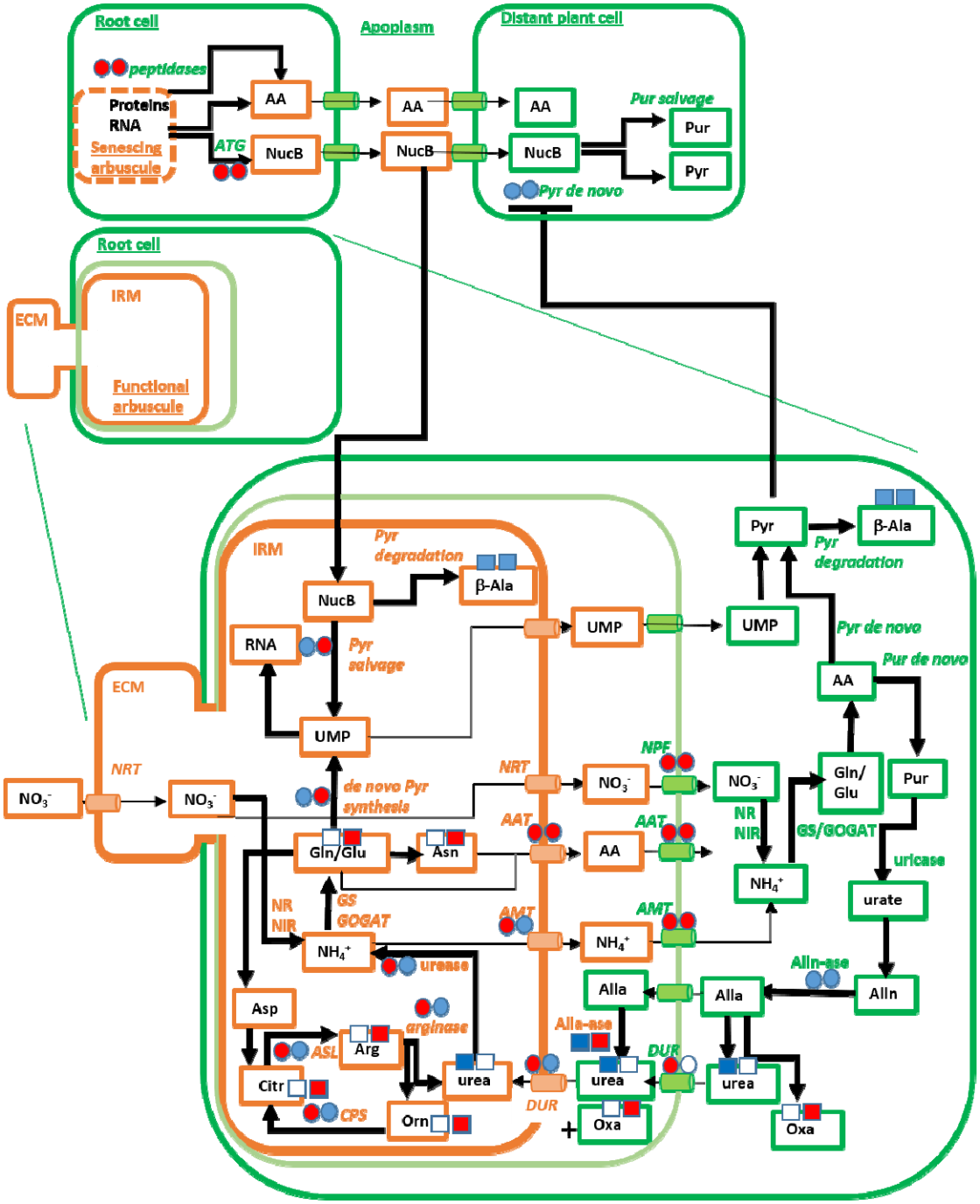

Figure 9: Hypothetical working model for maize and *R. irregularis* N nutrition under LN and HN. To build the model, the metabolomic data from B73 and Lo3 maize lines were pooled for simplification (Supplementary Figure 10) and we used genes in Supplementary Tables 7 and 8. In some cases genes with multigene families such as Glutamine Synthetase encoding genes have different expression profiles. For simplification purposes, these cases were not considered in the hypothetical mechanistic model below.

- Under LN fungal RNAseq data indicate up regulation of amino acid transporters (AAT) and ammonium transporters (AMT). Fungal argininosuccinate lyase (ASL) and arginase genes are up regulated under LN, which could lead to urea accumulation. A fungal urea transporter (*DUR*) is upregulated under LN, it is likely to be expressed in the IRM but could

also be expressed in the ECM. Usually DUR is an exporter of urea, it remains to be determined how this *R. irregularis* DUR transporters acts during AM symbiosis. However, urea is probably further degraded into ammonium by urease since the fungal urease coding gene is up regulated under LN. This could explain the fact that under LN, *R. irregularis* inoculated roots accumulate less urea. Globally lower amounts of amino acids are found in LN roots which suggests less assimilation via GS-GOGAT in the fungal and inoculated plant root cells. The fungal RNAseq data indicate that pyrimidine de novo biosynthetic genes are down regulated under LN compared to HN but still expressed (for example, UMP synthase, orototate phosphorybolsyl transferase) as well as the pyrimidine salvage pathway (for example, dUTPase, allantoicase, deoxycitydylate deaminase, cytosine deaminase). These data suggest that under LN, the fungus redirects its N metabolism in order to provide NH_4^+ to the plant cell, but may also provide nueclosides to plant cells.

- Under HN, high amounts of NO_3^- are available to the fungus and to the plant. Fungal RNAseq data indicate up-regulation of some amino acid transporters that are different from those up-regulated in LN, down regulation of ammonium permeases. Fungal argininosuccinate lyase and arginase genes are down-regulated under HN, which could lead to urea accumulation. A fungal urea transporter is down-regulated under HN. We observe a global increase in the amounts several amino acids including Citr, which is a precursor of Arg. Arg and Asn accumulate in inoculated roots indicating that fungal and/or and plant assimilation via GS-GOGAT are probably upregulated under HN in response to the fungus. The fungal RNAseq data indicate that in HN roots, pyrimidine de novo biosynthetic genes are up-regulated (for example, UMP synthase, orototate phosphorybolsyl transferase) as well as the pyrimidine salvage pathway (for example, dUTPase, allantoicase, deoxycitydylate deaminase, cytosine deaminase). Allantoin accumulates only in HN roots and not in LN roots, and its amount is not affected by inoculation in HN roots. Allantoin can be converted into allantoic acid which can be released in the apoplast. In HN roots a fungal allantoicase is up-regulated suggesting that urea is produced by this pathway under HN.
- In italics, genes. In boxes: metabolites. In orange : fungal genes or metabolites. In green : plant genes or metabolites. In front of genes and metabolites there are two squares. The square at the left indicates the status of the item under LN. The square at the right indicates the status of the item under HN. The circles at the left indicates the status of the gene expression under LN. The circle at the right indicates the status of the gene expression under HN. AA: Amino acids. NucB: Nucleobases. Pur: Purine. Pyr: Pyrimidine. IRM: Intraradical mycelium. ECM: Extraradical mycelium. .Alla: Allantoic Acid. Alln : Allantoin. Alln-ase: Allantoinase. Arg: arginine. Asn: Asparagine. Asp : Aspartate. b-Ala :b-alanine. Citr : Citrulline. Glu: Glutamate. Gln: Glutamine. Orn : Ornithine. GOGAT: Glutamine Oxo-Glutarate Aminotransferase. Oxa : Oxalic Acid. NR : Nitrate reductase. NiR : Nitrite reductase. AAT : Amino acid transporter. AMT : Ammonium transporter. DUR : Urea transporter. NPF : plant Nitrate transporter. NRT : R. irregularis nitrate transporter. CPS : Carbamoyl-phosphate synthase. ASL : Argininosuccinate lyase. Pyr de novo: Pyrimidine de novo biosynthetic pathway. Pur de novo: Pur de novo biosynthetic pathway.

Table 1 : **List of metabolic bottlenecks relieved and created by *R. irregularis* or N supply.** Metabolic bottlenecks were identified by MBA that are relieved by either R. irregularis treatment or HN treatment compared to LN control conditions are indicated as "debottlnecked". Those that were newly created following R. irregularis or HN treatment were compared to LN control conditions are indicated as "new metabolic" bottelnecks.

Reactions Debottelnecked by *R. irregularis* treatment	
R03817[M,t]	Photosynthesis light reactions
R00124[R,p]	Purine and Pyrimidine metabolism
R00692[R,p]	Phenylalanine, tyrosine, and tryptophan metabolism
R04241_mod[R,m]	Folate metabolism
Reactions Debottelnecked by HN treatment	
R03817[M,t]	Photosynthesis light reactions
R00124[R,p]	Purine Pyrimidine metabolism
R00692[R,p]	Phenylalanine, tyrosine, and tryptophan metabolism
R00095[R,x]	Ascorbate and aldarate metabolism
New metabolic bottlnecks with LN RHIZO	
R03346[M,c]	Nicotinate and nicotinamide metabolism
R03346[B,c]	Nicotinate and nicotinamide metabolism
R00086[M,pm]	Purine metabolism
R00986[R,p]	Purine metabolism
MR00968[B,c]	Benzoate metabolism
R00086[B,pm]	Purine metabolism
R00341[R,c]	Pyruvate metabolism
R00216[B,p]	Pyruvate metabolism
R01058[B,c]	Glycolysis
R02678[R,m]	Phenylalanine, tyrosine, and tryptophan metabolism
R00710[R,m]	Pyruvate metabolism
R01067[R,c]	Calvin-Benson-Bassham cycle
R01067[R,p]	Calvin-Benson-Bassham cycle
New bottlnecks in HN	
R00341[R,c]	Pyruvate metabolism
R00709_mod[R,m]	TCA cycle
R00713[R,m]	Alanine, aspartate, and glutamate metabolism
R01067[R,c]	Calvin-Benson-Bassham cycle
R01067[R,p]	Calvin-Benson-Bassham cycle
R01667[R,p]	Pyrimidine metabolism
R00235[B,x]	Pyruvate metabolism
R00885[B,c]	Fructose and mannose metabolism
R01058[B,c]	Glycolysis
R02080[M,c]	Phenylalanine, tyrosine, and tryptophan metabolism
R00214[M,m]	Pyruvate metabolism
R00124[B,p]	Purine metabolism
R00267_mod[M,c]	Alanine, aspartate, and glutamate metabolism

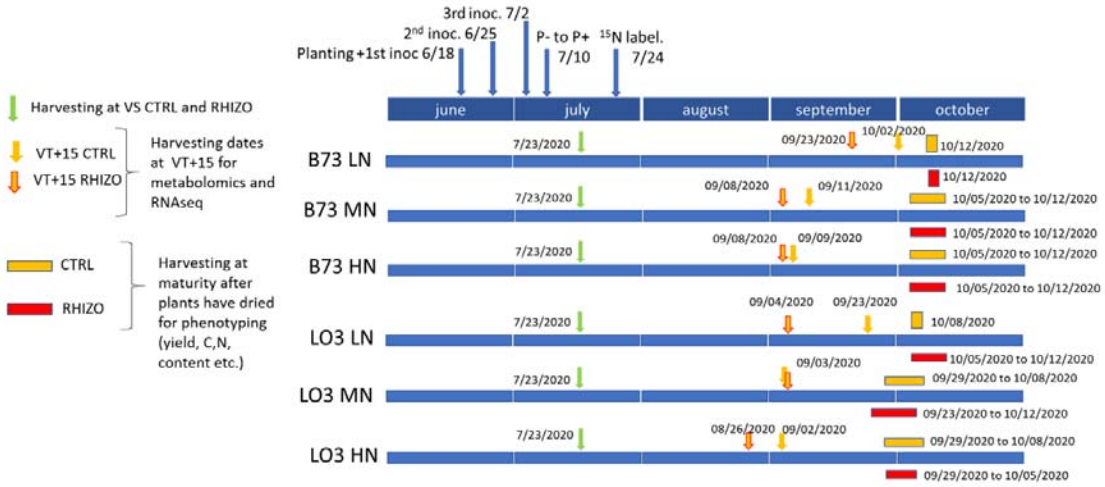

Supplementary Figure 1: Experimental design with dates of each treatment and harvesting. Experiments were performed at indicated dates during the summer of 2020 in the greenhouse. Each date is represented on the boxes below for each maize line/condition. For each maize line/condition, the harvesting dates for the vegetative stage (VS) and 15 days after vessel tasseling (VT+15) stage are indicated. The horizontal red and yellow boxes indicate the periodes of harvesting dry mature plants for physio-agronomical trait phenotyping. Ctrl: Mock non inoculated control. RHIZO: inoculated with *R. irregularis*.

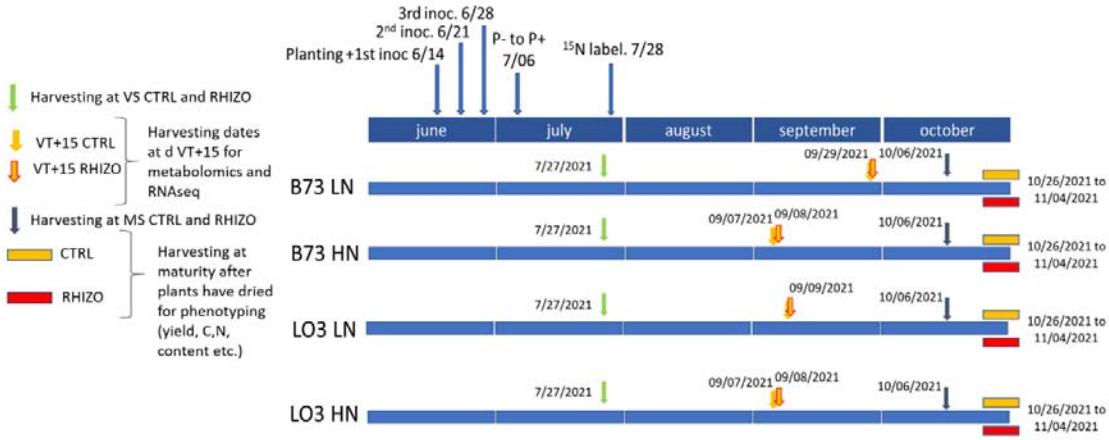

Supplementary Figure 2: Experimental design with details for dates of each treatment and harvesting dates. Experiments were performed at indicated dates during the summer of 2021 in the greenhouse. Each date is represented on the boxes below for each maize line/condition. For each maize line/condition, the harvesting dates for the vegetative stage (VS) and 15 days after vessel tasseling (VT+15) stage are indicated. The horizontal red and yellow boxes indicate the periodes of harvesting dry mature plants for physio-agronomical trait phenotyping. Ctrl: Mock non inoculated control. RHIZO: inoculated with *R. irregularis*.

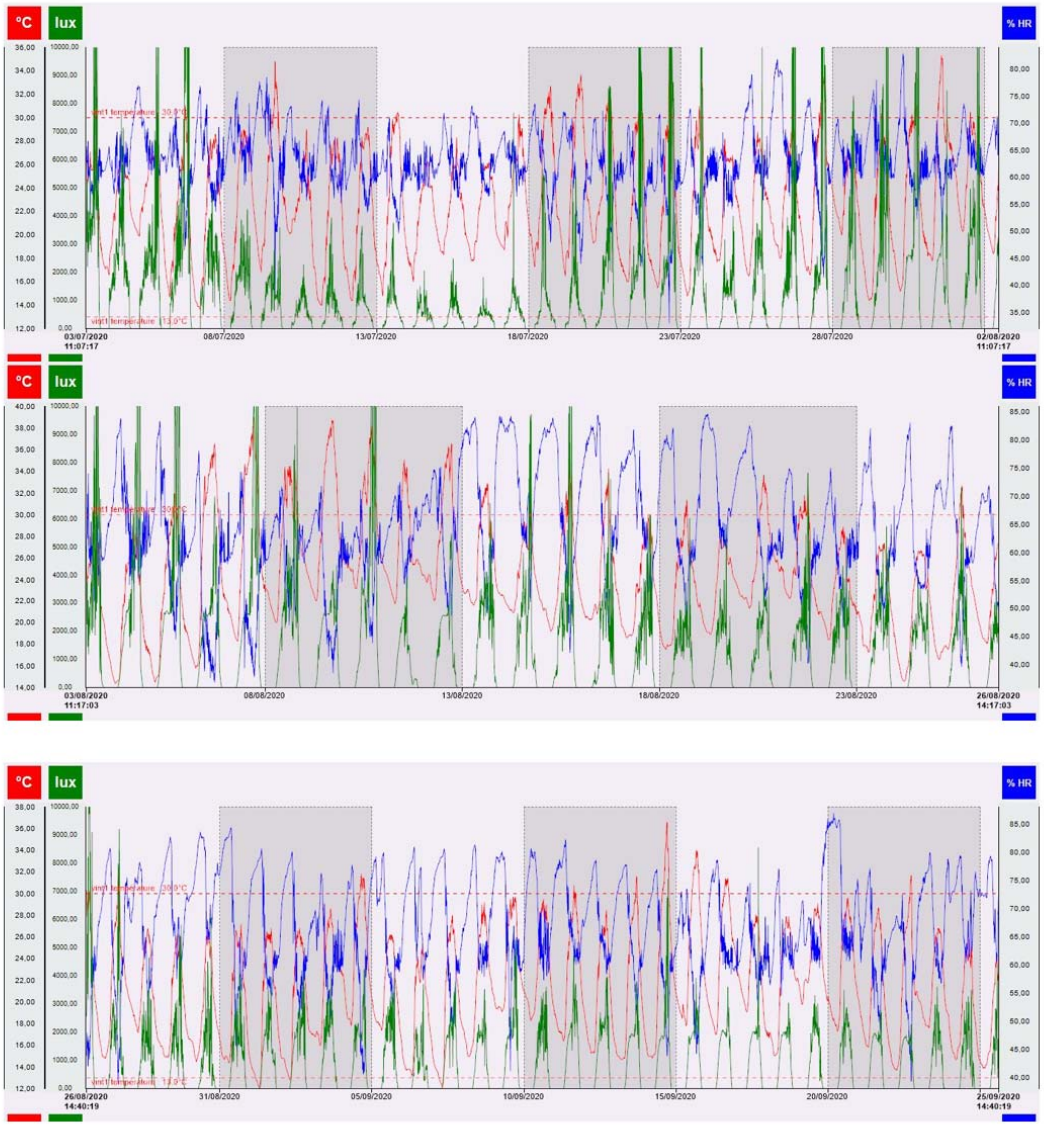

Supplementary Figure 3: Meteorological data collected in the greenhouse for the 2020 experiment (Supplementary Figure 1). In red the temperature in °C. In green the light intensity in Lux. In blue, the % of humidity. Data from July 3rd to September 26th 2020 are shown.

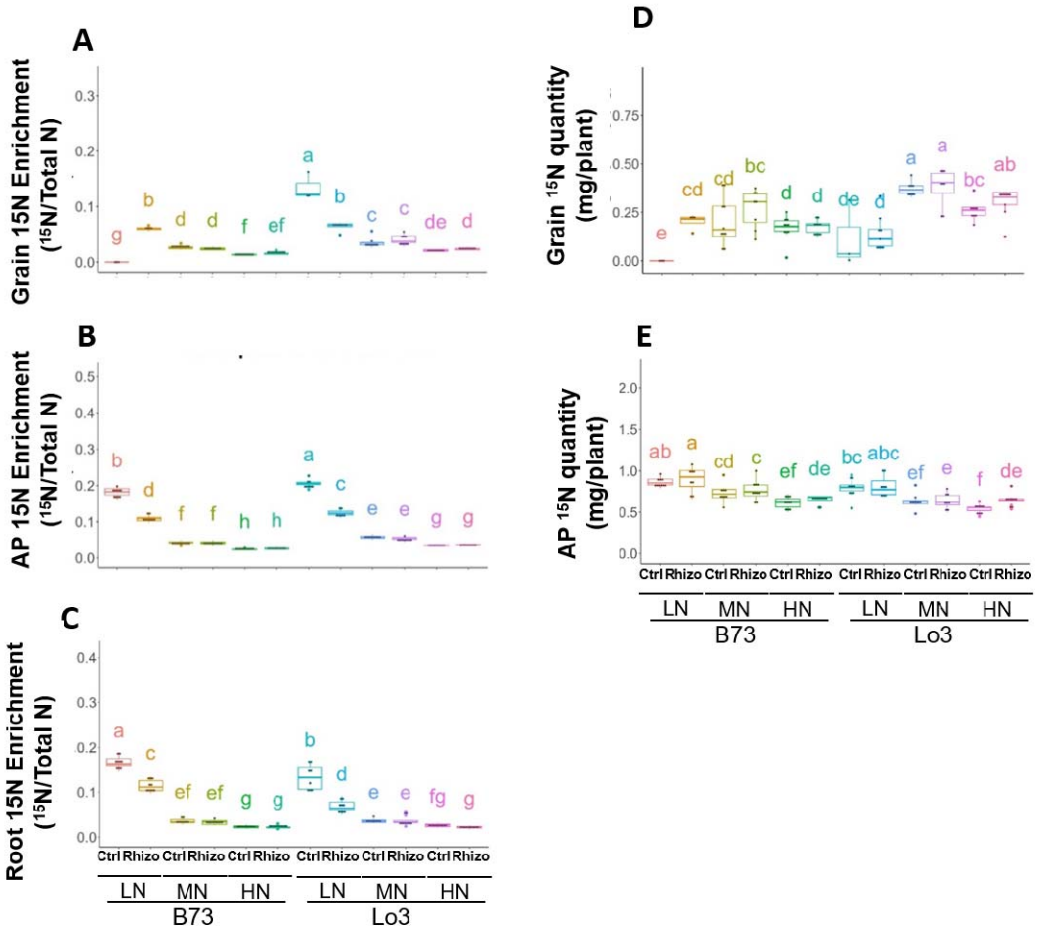

Supplementary Figure 4: Impact of N supply on N isotope fractionation and ^{15}N uptake in tresponse to *R. irregularis* shows that AM symbiosis and N supply hava a strong effect on N uptake. Plants were grown and harvested in 2020 as indicated in materials and methods under low nitrate (LN, 1mM NO_3^-), moderate nitrate (MN, 5mM NO_3^-) or high nitrate (HN, 10mM NO_3^-). Plants were subjected to a short pulse with a ^{15}N labelled nutrient solution (See Materials and Methods)**. A, B** and **C :** ^{15}N enrichment in grains, aerial parts (AP) and roots respectively. **D** and **E :** ^{15}N quantity in mg/plant in grains and AP respectively. Ctrl: Mock non inoculated control, Rhizo: inoculated with *R. irregularis,* AP: Biomass of Aerial Parts. N=7 to 10 plants. Different letters indicate significantly different averages for the considered trait by ANOVA N=7-10 plants for grains and aerial parts. N=5 for roots.

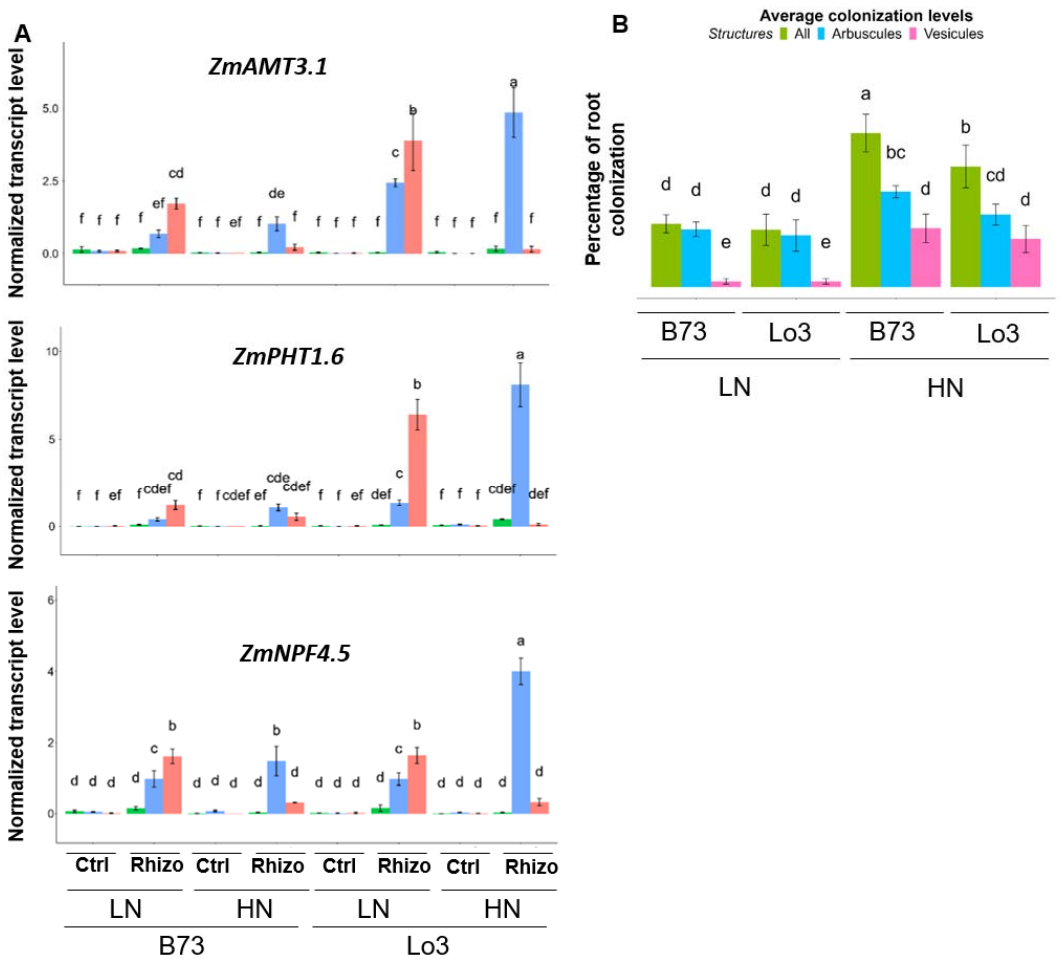

Supplementary Figure 5 : Impact of N supply on *R. irregularis* colonization and kinetics of symbiosis marker gene expression. Plants were grown and harvested in 2021 as indicated in materials and methods under low nitrate (LN, 1mM NO_3^-) or high nitrate (HN, 10mM NO_3^-). **A**: AM Symbiotic gene expression levels quantified by qRT-PCR. **B**: Quantification of root colonization level by microscopic observation of different fungal structures : arbuscules, vesicles and the global colonization level (All) in roots harvested at VT+15 stage. Ctrl: Mock non inoculated control, Rhizo: inoculated with *R. irregularis.* N=8. Bars indicate SD. Different letters indicate significantly different averages for the considered gene transcript level or trait by ANOVA.

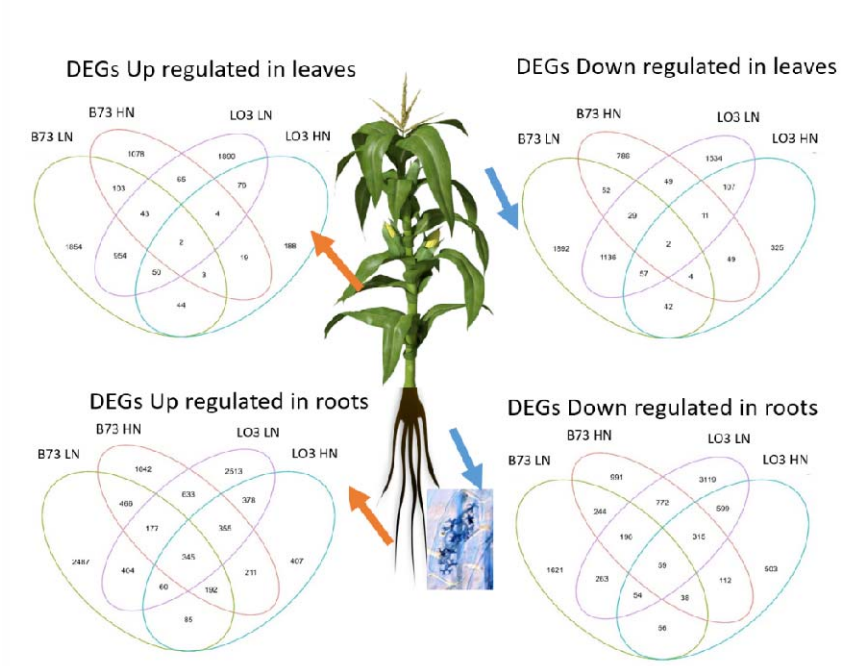

Supplementary Figure 6 : Venn diagram of RNAseq data showing the overlap between maize DEG under LN or HN in line B73 and LO3. Genes were selected so that their fold change (inoculated versus control) was > to 1.5 and statistically significant in the 3 replicates. B73 LN and B73 HN represent DEG genes up or down regulated in inoculated plants compared to control plants in LN or HN respectively; LO3 LN and LO3 HN represent DEG genes up or down regulated in inoculated plants compared to control plants in LN or HN respectively.

.

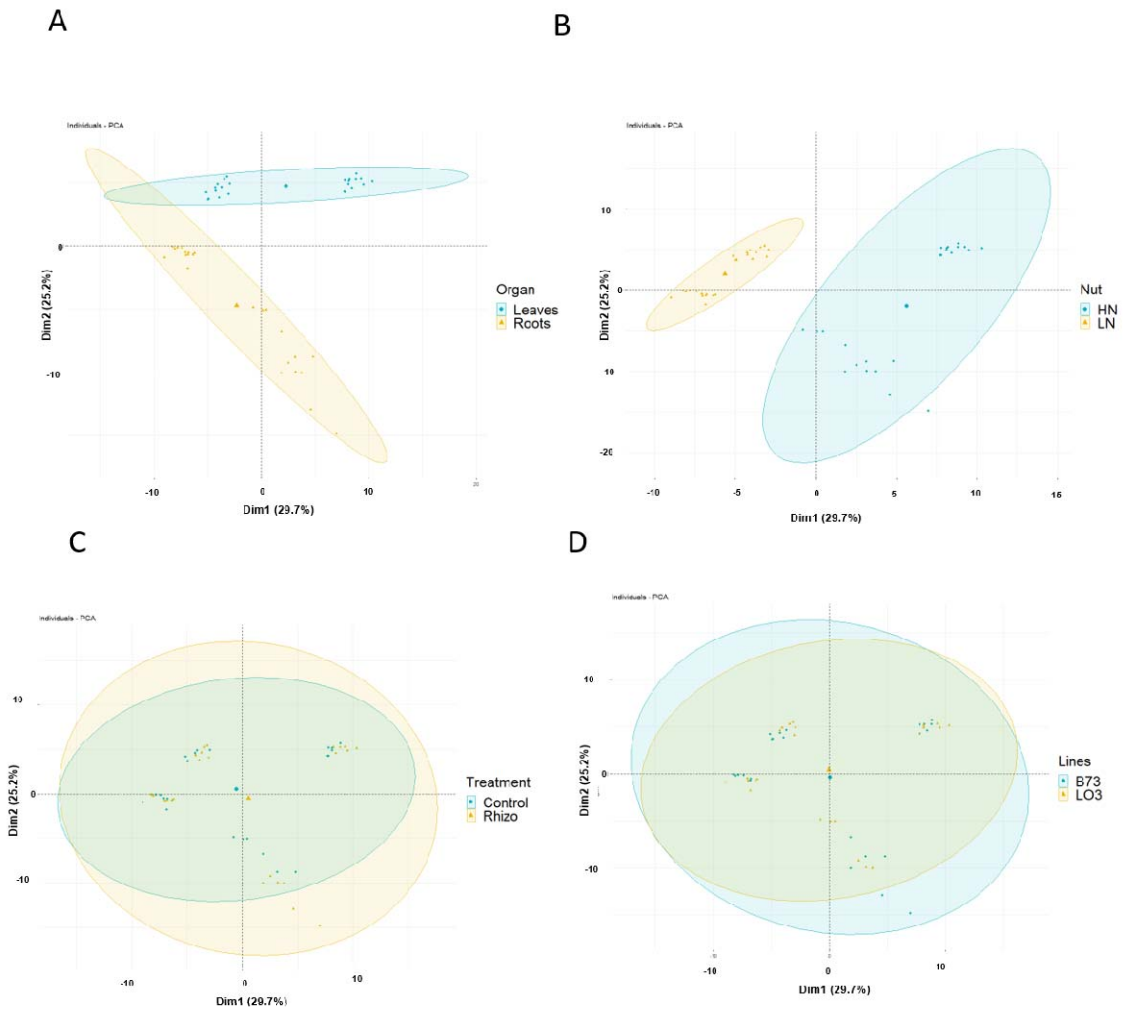

Supplementary Figure 7: PCA on metabolomics data showing different impacts of N nutrition, organ, maize genotype or R. irregularis inoculation on metabolome. Plants were grown and harvested in 2020 as indicated in materials and methods under low nitrate (LN, 1mM NO_3^-) or high nitrate (HN, 10mM NO_3^-) at VT+15 stage. Primary metabolite profiles obtained by GC/MS were used to build these PCAs from leaves and roots of inoculated (Rhizo) or mock non-inoculated control (Ctrl) plants under LN or HN from B73 and Lo3 genotypes.

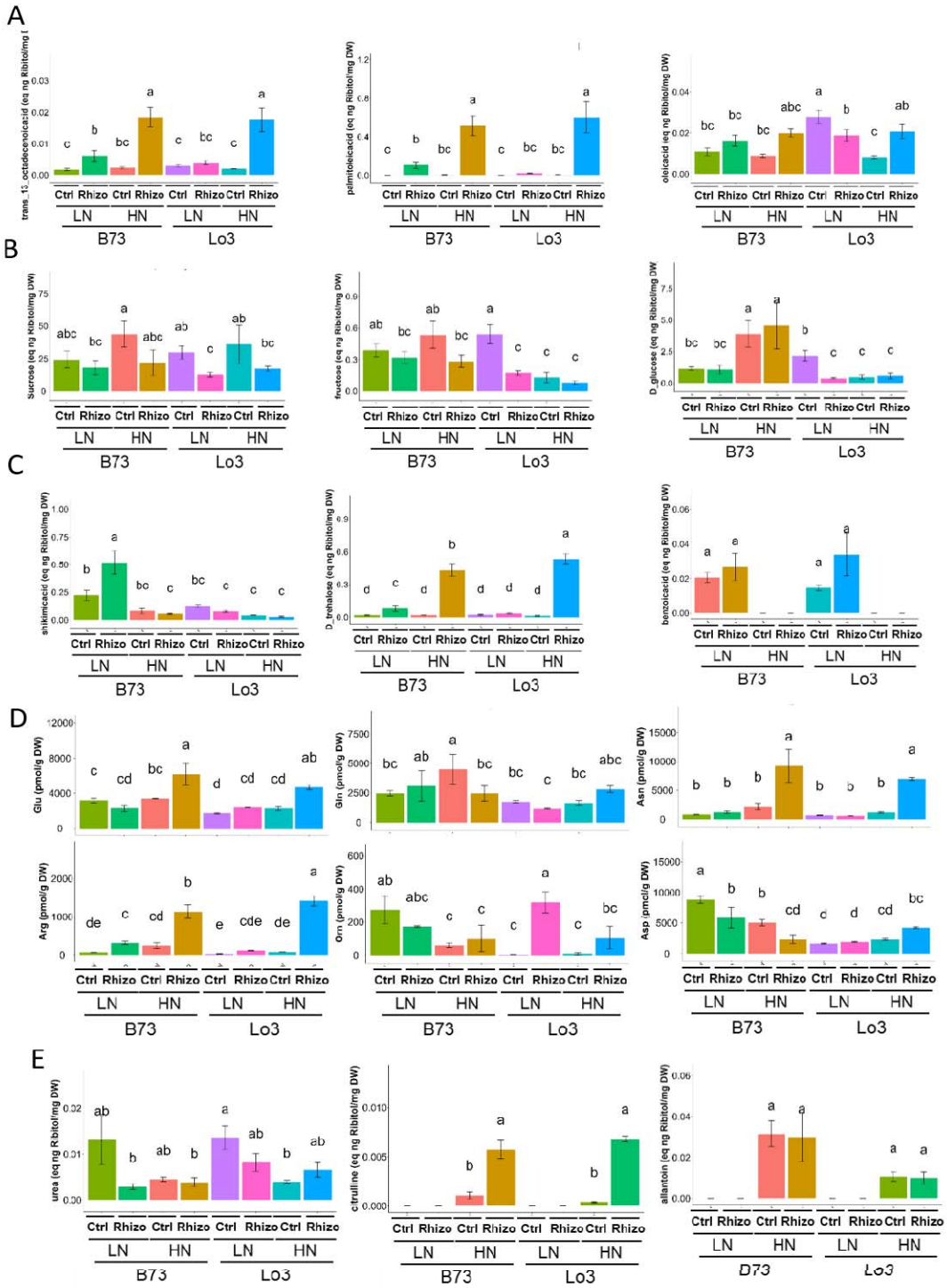

Supplementary Figure 8 : Examples of metabolites accumulating in roots in response to *R. irregularis*. Plants were grown and harvested in 2020 as indicated in materials and methods under low nitrate (LN, 1mM NO_3^-) or high nitrate (HN, 10mM NO_3^-). Roots were harvested at VT+15 stage. Ctrl: Mock non inoculated control, Rhizo: *R. irregularis,* N=3. Different letters indicate significantly different gene expression levels as analyzed by ANOVA. Bars are standard errors.. Metabolites were quantified in identified samples by GS/MS in A, B,C and E or HPLC in D. **A**: examples of lipids. **B**: examples of soluble sugars. **C**: Examples of defense related metabolites. **D and E**: examples of N related metabolites.

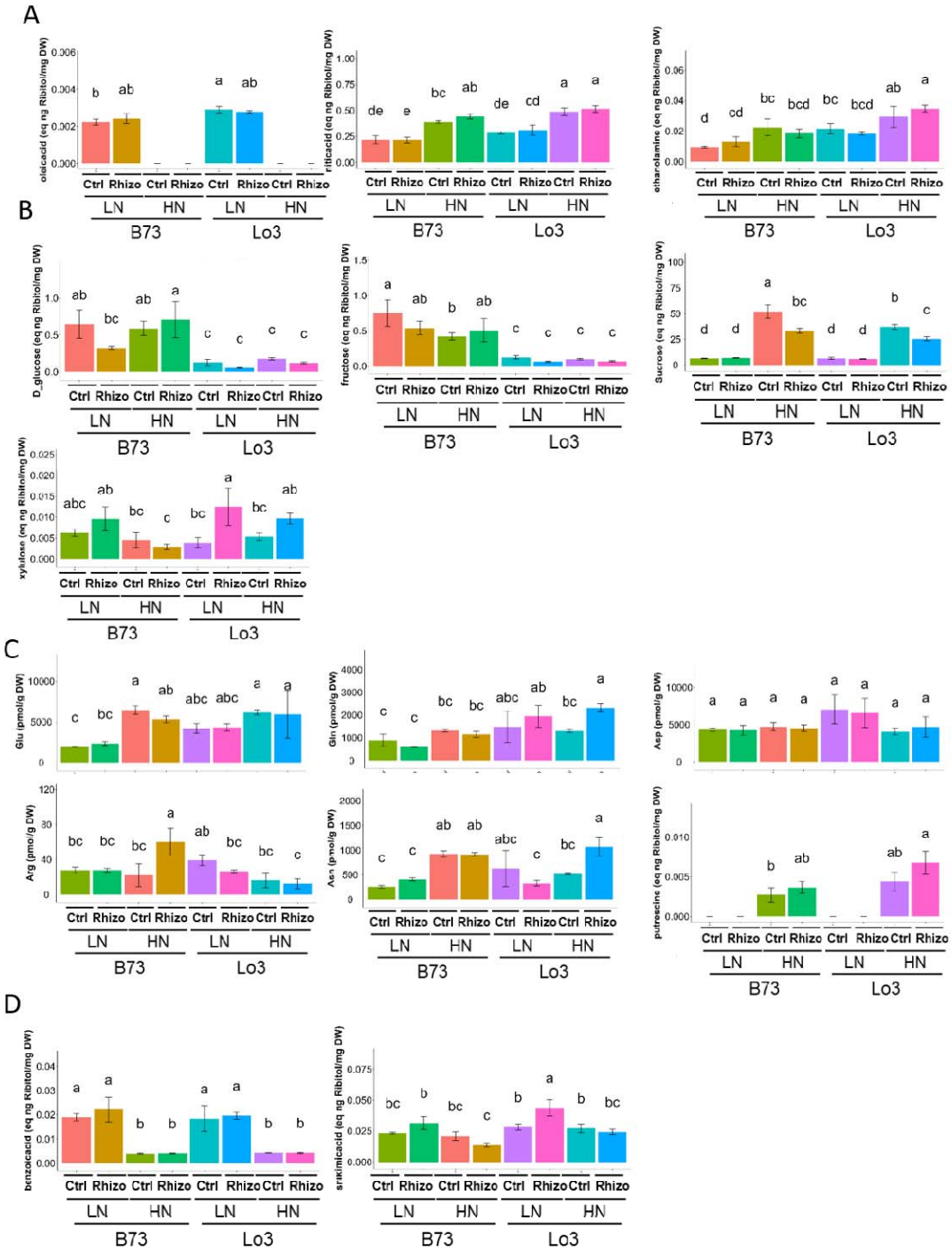

Supplementary Figure 9 : Examples of metabolites accumulating in leaves in response to *R. irregularis*. Plants were grown and harvested in 2020 as indicated in materials and methods under low nitrate (LN, 1mM NO_3^-) or high nitrate (HN, 10mM NO_3^-). Roots were harvested at VT+15 stage. Ctrl: Mock non inoculated control, R: inoculated with *R. irregularis,* N=3. Different letters indicate significantly different gene expression levels as analyzed by ANOVA. Bars are standard errors. Metabolites were quantified in indicated samples by GS/MS or HPLC. Metabolites monitored by GC/MS are indicated by relative abundance to ribitol. Metabolites quantified by HPLC are indicated by absolute quantities (pmol/g DW). **A**: examples of lipid related metabolites. **B**: examples of sugars. **C**: Examples of N related metabolites. **D** : Examples of defense related metabolites.

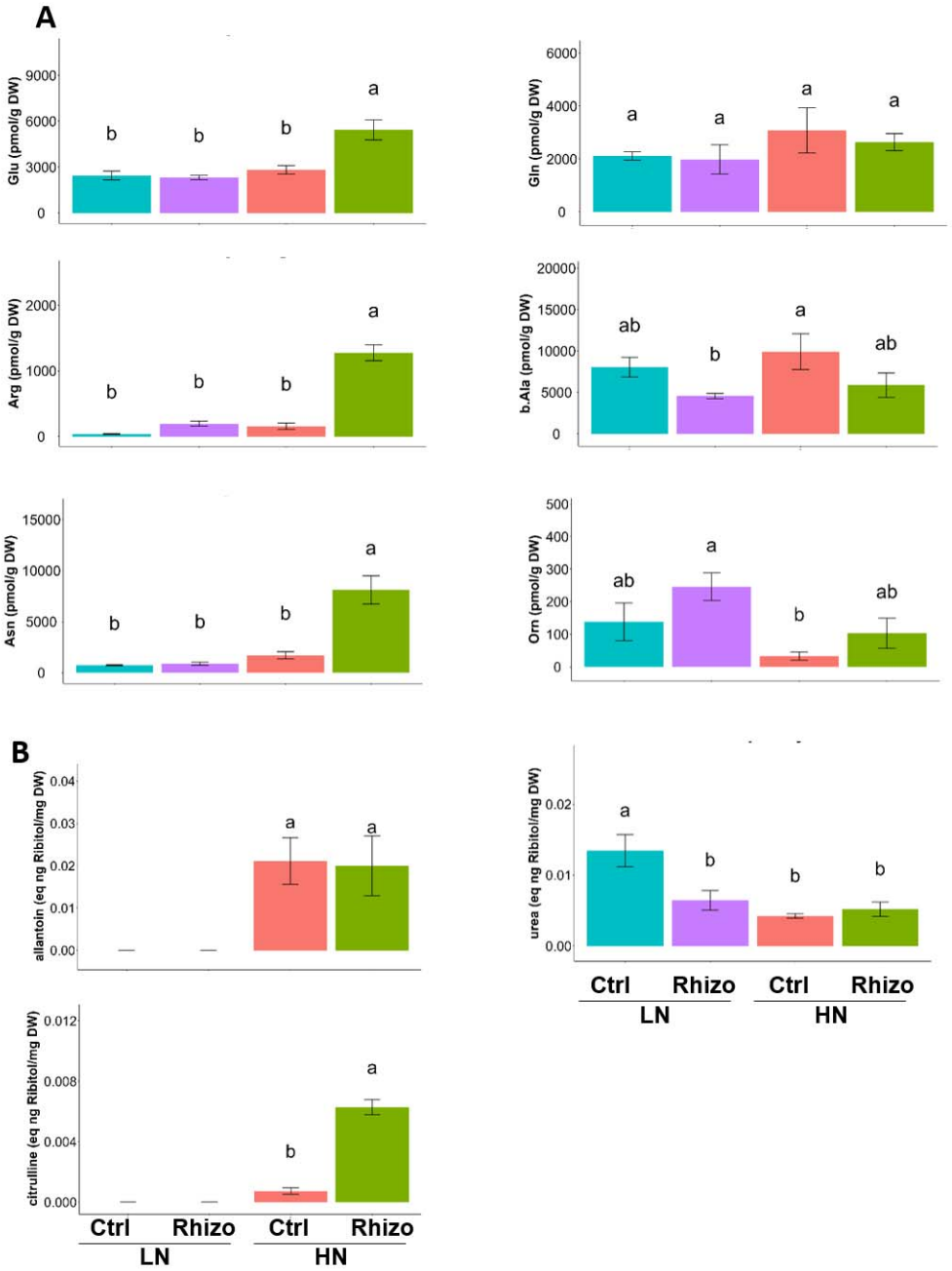

Supplementary Figure 10 : Metabolite profiles supporting hypothetical model in roots. Plants were grown and harvested in 2020 as indicated in materials and methods under low nitrate (LN, 1mM NO_3^-) or high nitrate (HN, 10mM NO_3^-). Roots were harvested at VT+15 stage. Metabolites related to the mecanistic hypothetical model in Figure 9 from both B73 and Lo3 maize lines were pooled. **A:** metabolites quantified by HPLC. In **B** metabolites monitored by GC/MS.Ctrl: Mock non inoculated plants. Rhizo: inoculated with *R. irregularis*.

References:

AU - Baudry K, AU - Paysant-Le Roux C, AU - Colella S, AU - Castandet B, AU - Martin M-L. 2022. Analyzing Multifactorial RNA-Seq Experiments with DiCoExpress. JoVE, e62566.

Balzergue C, Chabaud M, Barker D, Bécard G, Rochange S. 2013. High phosphate reduces host ability to develop arbuscular mycorrhizal symbiosis without affecting root calcium spiking responses to the fungus . Frontiers in Plant Science **4**.

BARROSO J, CASIMIRO A, CARRAPIÇO F, SLOMÉ M, PAIS S. 1988. Localization of uricase in mycorrhizas of Ophrys lutea Cav. New Phytologist **108**, 335–340.

Berger F, Gutjahr C. 2021. Factors affecting plant responsiveness to arbuscular mycorrhiza. Current Opinion in Plant Biology **59**, 101994.

Breuillin F, Schramm J, Hajirezaei M, *et al.* 2010. Phosphate systemically inhibits development of arbuscular mycorrhiza in Petunia hybrida and represses genes involved in mycorrhizal functioning. The Plant Journal **64**, 1002–1017.

Cañas RA, Yesbergenova-Cuny Z, Simons M, *et al.* 2017. Exploiting the Genetic Diversity of Maize Using a Combined Metabolomic, Enzyme Activity Profiling, and Metabolic Modeling Approach to Link Leaf Physiology to Kernel Yield. The Plant Cell **29**, 919–943.

Chen A, Gu M, Wang S, Chen J, Xu G. 2018*a*. Transport properties and regulatory roles of nitrogen in arbuscular mycorrhizal symbiosis. Seminars in Cell & Developmental Biology **74**, 80–88.

Chen ECH, Morin E, Beaudet D, *et al.* 2018*b*. High intraspecific genome diversity in the model arbuscular mycorrhizal symbiont Rhizophagus irregularis. New Phytologist **220**, 1161–

1171.

Cheng C-Y, Li Y, Varala K, *et al.* 2021. Evolutionarily informed machine learning enhances the power of predictive gene-to-phenotype relationships. Nature Communications **12**, 5627.

Choi J, Summers W, Paszkowski U. 2018. Mechanisms Underlying Establishment of Arbuscular Mycorrhizal Symbioses. Annual Review of Phytopathology **56**, 135–160.

Chowdhury NB, Alsiyabi A, Saha R. 2022*a*. Characterizing the Interplay of Rubisco and Nitrogenase Enzymes in Anaerobic-Photoheterotrophically Grown Rhodopseudomonas palustris CGA009 through a Genome-Scale Metabolic and Expression Model. Microbiology Spectrum **10**, e01463-22.

Chowdhury NB, Decouard B, Quillere I, *et al.* 2023. Multi-organ Metabolic Model of Zea mays Connects Temperature Stress with Thermodynamics-Reducing Power-Energy Generation Axis. bioRxiv, 2023.07.09.548275.

Chowdhury NB, Schroeder WL, Sarkar D, Amiour N, Quilleré I, Hirel B, Maranas CD, Saha R. 2022*b*. Dissecting the metabolic reprogramming of maize root under nitrogen-deficient stress conditions. Journal of Experimental Botany **73**, 275–291.

Courty PE, Smith P, Koegel S, Redecker D, Wipf D. 2015. Inorganic Nitrogen Uptake and Transport in Beneficial Plant Root-Microbe Interactions. Critical Reviews in Plant Sciences **34**, 4–16.

Das D, Paries M, Hobecker K, Gigl M, Dawid C, Lam H-M, Zhang J, Chen M, Gutjahr C. 2022. PHOSPHATE STARVATION RESPONSE transcription factors enable arbuscular mycorrhiza symbiosis. Nature Communications **13**, 477.

Dechorgnat J, Francis KL, Dhugga KS, Rafalski JA, Tyerman SD, Kaiser BN. 2019. Tissue and nitrogen-linked expression profiles of ammonium and nitrate transporters in maize. BMC Plant Biology **19**, 206.

Dellagi A, Quillere I, Hirel B. 2020. Beneficial soil-borne bacteria and fungi: a promising

way to improve plant nitrogen acquisition. Journal of Experimental Botany **71**, 4469–4479.

Dobin A, Davis CA, Schlesinger F, Drenkow J, Zaleski C, Jha S, Batut P, Chaisson M, Gingeras TR. 2013. STAR: ultrafast universal RNA-seq aligner. Bioinformatics **29**, 15–21.

Fan X, Naz M, Fan X, Xuan W, Miller AJ, Xu G. 2017. Plant nitrate transporters: from gene function to application. Journal of Experimental Botany **68**, 2463–2475.

Fernie AR, Bachem CWB, Helariutta Y, *et al.* 2020. Synchronization of developmental, molecular and metabolic aspects of source–sink interactions. Nature Plants **6**, 55–66.

Fiehn O. 2006. Metabolite Profiling in Arabidopsis BT - Arabidopsis Protocols. In: Salinas J,, In: Sanchez-Serrano JJ, eds. Totowa, NJ: Humana Press, 439–447.

Fiehn O, Wohlgemuth G, Scholz M, Kind T, Lee DY, Lu Y, Moon S, Nikolau B. 2008. Quality control for plant metabolomics: reporting MSI-compliant studies. The Plant Journal **53**, 691–704.

Fiorilli V, Catoni M, Miozzi L, Novero M, Accotto GP, Lanfranco L. 2009. Global and cell-type gene expression profiles in tomato plants colonized by an arbuscular mycorrhizal fungus. New Phytologist **184**, 975–987.

Gagnot S, Tamby J-P, Martin-Magniette M-L, Bitton F, Taconnat L, Balzergue S, Aubourg S, Renou J-P, Lecharny A, Brunaud V. 2008. CATdb: a public access to Arabidopsis transcriptome data from the URGV-CATMA platform. Nucleic Acids Research **36**, D986–D990.

Galili T, O'Callaghan A, Sidi J, Sievert C. 2018. heatmaply: an R package for creating interactive cluster heatmaps for online publishing. Bioinformatics **34**, 1600–1602.

Gallou A, Declerck S, Cranenbrouck S. 2012. Transcriptional regulation of defence genes and involvement of the WRKY transcription factor in arbuscular mycorrhizal potato root colonization. Functional & Integrative Genomics **12**, 183–198.

Garcia K, Doidy J, Zimmermann SD, Wipf D, Courty P-E. 2016. Take a Trip Through the

Plant and Fungal Transportome of Mycorrhiza. Trends in Plant Science **21**, 937–950.

Gianinazzi S, Gollotte A, Binet M-N, van Tuinen D, Redecker D, Wipf D. 2010. Agroecology: the key role of arbuscular mycorrhizas in ecosystem services. Mycorrhiza **20**, 519–530.

Giovannetti M, Mosse B. 1980. An Evaluation of Techniques for Measuring Vesicular Arbuscular Mycorrhizal Infection in Roots. The New Phytologist **84**, 489–500.

Gojon A. 2022. Nitrogen acquisition in arbuscular mycorrhizal symbioses: A step into the real world. Journal of Plant Physiology **271**, 153646.

Grandclaudon M, Perrot-Dockès M, Trichot C, *et al.* 2019. A Quantitative Multivariate Model of Human Dendritic Cell-T Helper Cell Communication. Cell **179**, 432-447.e21.

Handa Y, Nishide H, Takeda N, Suzuki Y, Kawaguchi M, Saito K. 2015. RNA-seq Transcriptional Profiling of an Arbuscular Mycorrhiza Provides Insights into Regulated and Coordinated Gene Expression in Lotus japonicus and Rhizophagus irregularis. Plant and Cell Physiology **56**, 1490–1511.

Hirel B, Le Gouis J, Ney B, Gallais A. 2007. The challenge of improving nitrogen use efficiency in crop plants: Towards a more central role for genetic variability and quantitative genetics within integrated approaches. Journal of Experimental Botany.

Hirel B, Krapp ABT-RM in LS. 2020. Nitrogen Utilization in Plants I Biological and Agronomic Importance. Elsevier, .

Hirel B, Tétu T, Lea PJ, Dubois F. 2011. Improving Nitrogen Use Efficiency in Crops for Sustainable Agriculture. Sustainability **3**.

Hui J, An X, Li Z, *et al.* 2022. The mycorrhiza-specific ammonium transporter ZmAMT3;1 mediates mycorrhiza-dependent nitrogen uptake in maize roots. The Plant Cell **34**, 4066–4087.

Hull R, Choi J, Paszkowski U. 2021. Conditioning plants for arbuscular mycorrhizal

symbiosis through DWARF14-LIKE signalling. Current Opinion in Plant Biology **62**, 102071.

Ingraffia R, Amato G, Sosa-Hernández MA, Frenda AS, Rillig MC, Giambalvo D. 2020. Nitrogen Type and Availability Drive Mycorrhizal Effects on Wheat Performance, Nitrogen Uptake and Recovery, and Production Sustainability . Frontiers in Plant Science **11**, 760.

Kant S. 2018. Understanding nitrate uptake, signaling and remobilisation for improving plant nitrogen use efficiency. Seminars in Cell & Developmental Biology **74**, 89–96.

Kaur S, Suseela V. 2020. Unraveling Arbuscular Mycorrhiza-Induced Changes in Plant Primary and Secondary Metabolome. Metabolites **10**.

Keymer A, Pimprikar P, Wewer V, *et al.* 2017. Lipid transfer from plants to arbuscular mycorrhiza fungi (G Stacey, Ed.). eLife **6**, e29107.

Kopylova E, Noé L, Touzet H. 2012. SortMeRNA: fast and accurate filtering of ribosomal RNAs in metatranscriptomic data. Bioinformatics **28**, 3211–3217.

Krapp A, David LC, Chardin C, Girin T, Marmagne A, Leprince AS, Chaillou S, Ferrario-Méry S, Meyer C, Daniel-Vedele F. 2014. Nitrate transport and signalling in Arabidopsis. Journal of Experimental Botany.

Lambert I, Paysant-Le Roux C, Colella S, Martin-Magniette M-L. 2020. DiCoExpress: a tool to process multifactorial RNAseq experiments from quality controls to co-expression analysis through differential analysis based on contrasts inside GLM models. Plant Methods **16**, 68.

Lanfranco L, Fiorilli V, Gutjahr C. 2018. Partner communication and role of nutrients in the arbuscular mycorrhizal symbiosis. New Phytologist **220**, 1031–1046.

Lassaletta L, Billen G, Garnier J, Bouwman L, Velazquez E, Mueller ND, Gerber JS. 2016. Nitrogen use in the global food system: past trends and future trajectories of agronomic performance, pollution, trade, and dietary demand. Environmental Research Letters **11**, 095007.

Lea PJ, Miflin BJ. 2018. Nitrogen Assimilation and its Relevance to Crop Improvement. Annual Plant Reviews online, 1–40.

Lee D-K, Redillas MCFR, Jung H, Choi S, Kim YS, Kim J-K. 2018. A Nitrogen Molecular Sensing System, Comprised of the ALLANTOINASE and UREIDE PERMEASE 1 Genes, Can Be Used to Monitor N Status in Rice . Frontiers in Plant Science **9**.

Li F, Chung T, Pennington JG, Federico ML, Kaeppler HF, Kaeppler SM, Otegui MS, Vierstra RD. 2015. Autophagic Recycling Plays a Central Role in Maize Nitrogen Remobilization. The Plant Cell **27**, 1389–1408.

Liu J, Fernie AR, Yan J. 2020. The Past, Present, and Future of Maize Improvement: Domestication, Genomics, and Functional Genomic Routes toward Crop Enhancement. Plant Communications **1**, 100010.

Liu Q, Wu K, Song W, Zhong N, Wu Y, Fu X. 2022. Improving Crop Nitrogen Use Efficiency Toward Sustainable Green Revolution. Annual Review of Plant Biology **73**, 523–551.

MacLean AM, Bravo A, Harrison MJ. 2017. Plant Signaling and Metabolic Pathways Enabling Arbuscular Mycorrhizal Symbiosis. The Plant Cell **29**, 2319–2335.

Masclaux-Daubresse C, Chen Q, Havé M. 2017. Regulation of nutrient recycling via autophagy. Current Opinion in Plant Biology **39**, 8–17.

Masclaux-Daubresse C, Daniel-Vedele F, Dechorgnat J, Chardon F, Gaufichon L, Suzuki A. 2010. Nitrogen uptake, assimilation and remobilization in plants: Challenges for sustainable and productive agriculture. Annals of Botany.

Masson-Boivin C, Sachs JL. 2018. Symbiotic nitrogen fixation by rhizobia—the roots of a success story. Current Opinion in Plant Biology **44**, 7–15.

McCarthy DJ, Chen Y, Smyth GK. 2012. Differential expression analysis of multifactor RNA-Seq experiments with respect to biological variation. Nucleic Acids Research **40**, 4288–4297.

Melino VJ, Tester MA, Okamoto M. 2022. Strategies for engineering improved nitrogen use efficiency in crop plants via redistribution and recycling of organic nitrogen. Current Opinion in Biotechnology **73**, 263–269.

Menadue DJ, Riboni M, Baumann U, Schilling RK, Plett DC, Roy SJ. 2021. Proton-pumping pyrophosphatase homeolog expression is a dynamic trait in bread wheat (Triticum aestivum). Plant Direct **5**, e354.

Meng L, Zhang A, Wang F, Han X, Wang D, Li S. 2015. Arbuscular mycorrhizal fungi and rhizobium facilitate nitrogen uptake and transfer in soybean/maize intercropping system . Frontiers in Plant Science **6**.

Morris DS, Chowdhury NB, Kathol M, Saha R. 2023. Opening the door to nitrogen fixation in oxygenic phototrophs. Trends in Biotechnology **41**, 283–285.

Murphy J, Riley JP. 1962. A modified single solution method for the determination of phosphate in natural waters. Analytica Chimica Acta **27**, 31–36.

Murtagh F, Legendre P. 2014. Ward's Hierarchical Agglomerative Clustering Method: Which Algorithms Implement Ward's Criterion? Journal of Classification **31**, 274–295.

Nanjareddy K, Arthikala M-K, Gómez B-M, Blanco L, Lara M. 2017. Differentially expressed genes in mycorrhized and nodulated roots of common bean are associated with defense, cell wall architecture, N metabolism, and P metabolism. PLOS ONE **12**, e0182328.

Paries M, Gutjahr C. 2023. The good, the bad, and the phosphate: regulation of beneficial and detrimental plant–microbe interactions by the plant phosphate status. New Phytologist **239**, 29–46.

Perrot-Dockès M, Lévy-Leduc C, Rajjou L. 2022. Estimation of Large Block Structured Covariance Matrices: Application to 'Multi-Omic' Approaches to Study Seed Quality. Journal of the Royal Statistical Society Series C: Applied Statistics **71**, 119–147.

Perrot-Dockès M, Lévy-Leduc C, Sansonnet L, Chiquet J. 2018. Variable selection in

multivariate linear models with high-dimensional covariance matrix estimation. Journal of Multivariate Analysis **166**, 78–97.

Plassard C, Becquer A, Garcia K. 2019. Phosphorus Transport in Mycorrhiza: How Far Are We? Trends in Plant Science **24**, 794–801.

Prioul J-L, Schwebel-Dugué N. 1992. Source-Sink Manipulations and Carbohydrate Metabolism in Maize. Crop Science **32**, cropsci1992.0011183X003200030035x.

Quiroga G, Erice G, Aroca R, Delgado-Huertas A, Ruiz-Lozano JM. 2020. Elucidating the Possible Involvement of Maize Aquaporins and Arbuscular Mycorrhizal Symbiosis in the Plant Ammonium and Urea Transport under Drought Stress Conditions. Plants **9**.

Ramírez-Flores MR, Bello-Bello E, Rellán-Álvarez R, Sawers RJH, Olalde-Portugal V. 2019. Inoculation with the mycorrhizal fungus Rhizophagus irregularis modulates the relationship between root growth and nutrient content in maize (Zea mays ssp. mays L.). Plant Direct **3**, e00192.

Ranum P, Peña-Rosas JP, Garcia-Casal MN. 2014. Global maize production, utilization, and consumption. Annals of the New York Academy of Sciences **1312**, 105–112.

Revilla P, Alves ML, Andelković V, *et al.* 2022. Traditional Foods From Maize (Zea mays L.) in Europe . Frontiers in Nutrition **8**.

Rigaill G, Balzergue S, Brunaud V, *et al.* 2018. Synthetic data sets for the identification of key ingredients for RNA-seq differential analysis. Briefings in Bioinformatics **19**, 65–76.

Robinson MD, McCarthy DJ, Smyth GK. 2010. edgeR: a Bioconductor package for differential expression analysis of digital gene expression data. Bioinformatics **26**, 139–140.

Sawers RJH, Ramírez-Flores MR, Olalde-Portugal V, Paszkowski U. 2018*a*. The impact of domestication and crop improvement on arbuscular mycorrhizal symbiosis in cereals: insights from genetics and genomics. New Phytologist **220**, 1135–1140.

Sawers RJHH, Ramírez-Flores MR, Olalde-Portugal V, Paszkowski U. 2018*b*. The impact

of domestication and crop improvement on arbuscular mycorrhizal symbiosis in cereals: insights from genetics and genomics. New Phytologist **220**, 1135–1140.

Sawers RJH, Svane SF, Quan C, *et al.* 2017. Phosphorus acquisition efficiency in arbuscular mycorrhizal maize is correlated with the abundance of root-external hyphae and the accumulation of transcripts encoding PHT1 phosphate transporters. New Phytologist **214**, 632–643.

Schaarschmidt S, Gresshoff PM, Hause B. 2013. Analyzing the soybean transcriptome during autoregulation of mycorrhization identifies the transcription factors GmNF-YA1a/b as positive regulators of arbuscular mycorrhization. Genome Biology **14**, R62.

Schlesinger WH. 2009. On the fate of anthropogenic nitrogen. Proceedings of the National Academy of Sciences **106**, 203 LP – 208.

Schmidt JE, Bowles TM, Gaudin ACM. 2016. Using Ancient Traits to Convert Soil Health into Crop Yield: Impact of Selection on Maize Root and Rhizosphere Function . Frontiers in Plant Science **7**.

Schnable PS, Ware D, Fulton RS, *et al.* 2009. The B73 Maize Genome: Complexity, Diversity, and Dynamics. Science **326**, 1112–1115.

Simons M, Saha R, Guillard L, Clément G, Armengaud P, Cañas R, Maranas CD, Lea PJ, Hirel B. 2014. Nitrogen-use efficiency in maize (Zea mays L.): From 'omics' studies to metabolic modelling. Journal of Experimental Botany **65**, 5657–5671.

Smith SE, Jakobsen I, Grønlund M, Smith FA. 2011. Roles of Arbuscular Mycorrhizas in Plant Phosphorus Nutrition: Interactions between Pathways of Phosphorus Uptake in Arbuscular Mycorrhizal Roots Have Important Implications for Understanding and Manipulating Plant Phosphorus Acquisition. Plant Physiology **156**, 1050–1057.

Smith SE, Read DJ. 2002. Mineral nutrition, heavy metal accumulation and water relations of VA mycorrhizal plants. Mycorrhizal Symbiosis, 126–160.

Su H, Cao Y, Ku L, *et al.* 2018. Dual functions of ZmNF-YA3 in photoperiod-dependent flowering and abiotic stress responses in maize. Journal of Experimental Botany **69**, 5177–5189.

Tegeder M. 2014. Transporters involved in source to sink partitioning of amino acids and ureides: opportunities for crop improvement. Journal of Experimental Botany **65**, 1865–1878.

Thakur K, Garg N. 2023. Differential Role of Silicon and Rhizoglomus intraradices in Modulating Amide and Ureide Metabolism of Seasonally Different Legume Species Subjected to Nickel Toxicity. Silicon.

Tisserant E, Malbreil M, Kuo A, *et al.* 2013. Genome of an arbuscular mycorrhizal fungus provides insight into the oldest plant symbiosis. Proceedings of the National Academy of Sciences **110**, 20117–20122.

Udvardi M, Poole PS. 2013. Transport and Metabolism in Legume-Rhizobia Symbioses. Annual Review of Plant Biology **64**, 781–805.

Urrutia M, Blein-Nicolas M, Fernandez O, Bernillon S, Maucourt M, Deborde C, Balliau T, Rabier D, Bénard C, Prigent S. 2023. Identification of metabolic and protein markers representative of the impact of mild nitrogen deficit on agronomic performance of maize hybrids.

Vangelisti A, Natali L, Bernardi R, Sbrana C, Turrini A, Hassani-Pak K, Hughes D, Cavallini A, Giovannetti M, Giordani T. 2018. Transcriptome changes induced by arbuscular mycorrhizal fungi in sunflower (Helianthus annuus L.) roots. Scientific Reports **8**, 4.

Verly C, Djoman ACR, Rigault M, Giraud F, Rajjou L, Saint-Macary ME, Dellagi A. 2020. Plant Defense Stimulator Mediated Defense Activation Is Affected by Nitrate Fertilization and Developmental Stage in Arabidopsis thaliana. Frontiers in Plant Science.

Verzeaux J, Hirel B, Dubois F, Lea PJ, Tétu T. 2017. Agricultural practices to improve

nitrogen use efficiency through the use of arbuscular mycorrhizae: Basic and agronomic aspects. Plant Science **264**, 48–56.

Wang S, Chen A, Xie K, *et al.* 2020. Functional analysis of the OsNPF4.5 nitrate transporter reveals a conserved mycorrhizal pathway of nitrogen acquisition in plants. Proceedings of the National Academy of Sciences **117**, 16649 LP – 16659.

Wang Y-Y, Cheng Y-H, Chen K-E, Tsay Y-F. 2018. Nitrate Transport, Signaling, and Use Efficiency. Annual Review of Plant Biology **69**, 85–122.

Wang W, Shi J, Xie Q, Jiang Y, Yu N, Wang E. 2017. Nutrient Exchange and Regulation in Arbuscular Mycorrhizal Symbiosis. Molecular Plant **10**, 1147–1158.

Wang E, Yu N, Bano SA, *et al.* 2014. A H+-ATPase That Energizes Nutrient Uptake during Mycorrhizal Symbioses in Rice and Medicago truncatula . The Plant Cell **26**, 1818–1830.

Wani SH, Vijayan R, Choudhary M, Kumar A, Zaid A, Singh V, Kumar P, Yasin JK. 2021. Nitrogen use efficiency (NUE): elucidated mechanisms, mapped genes and gene networks in maize (Zea mays L.). Physiology and Molecular Biology of Plants **27**, 2875–2891.

Wipf D, Krajinski F, van Tuinen D, Recorbet G, Courty P-E. 2019. Trading on the arbuscular mycorrhiza market: from arbuscules to common mycorrhizal networks. New Phytologist **223**, 1127–1142.

Witte CP, Herde M. 2020*a*. Nucleotide metabolism in plants. Plant Physiology **182**, 63–78.

Witte C-P, Herde M. 2020*b*. Nucleotide Metabolism in Plants1 [OPEN]. Plant Physiology **182**, 63–78.

Xie K, Ren Y, Chen A, Yang C, Zheng Q, Chen J, Wang D, Li Y, Hu S, Xu G. 2022. Plant nitrogen nutrition: The roles of arbuscular mycorrhizal fungi. Journal of Plant Physiology **269**, 153591.

Yonekura-Sakakibara K, Kojima M, Yamaya T, Sakakibara H. 2004. Molecular Characterization of Cytokinin-Responsive Histidine Kinases in Maize. Differential Ligand

Preferences and Response to cis-Zeatin. Plant Physiology **134**, 1654–1661.

Yooyongwech S, Threeprom W, Tisarum R, Samphumphuang T, Chungloo D, Cha-um S. 2022. Matching of Nitrogen Enhancement and Photosynthetic Efficiency by Arbuscular Mycorrhiza in Maize (Zea mays L.) in Relation to Organic Fertilizer Type. Plants **11**.

Zrenner R, Stitt M, Sonnewald U, Boldt R. 2006. PYRIMIDINE AND PURINE BIOSYNTHESIS AND DEGRADATION IN PLANTS. Annual Review of Plant Biology **57**, 805–836.